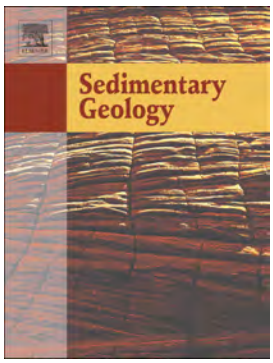

Fe-rich microspheres pseudomorphs after pyrite framboids in Holocene fluvial deposits from NE Spain: Relationship with environmental conditions and bacterial activity

María José Mayayo, Alfonso Yuste, Aránzazu Luzón, Alfonso Corzo, Arsenio Muñoz, Antonio Pérez, Asunción Soriano

PII: S0037-0738(19)30091-0
DOI: https://doi.org/10.1016/j.sedgeo.2019.04.003
Reference: SEDGEO 5480

To appear in: *Sedimentary Geology*

Received date: 17 January 2019
Revised date: 4 April 2019
Accepted date: 5 April 2019

Please cite this article as: M.J. Mayayo, A. Yuste, A. Luzón, et al., Fe-rich microspheres pseudomorphs after pyrite framboids in Holocene fluvial deposits from NE Spain: Relationship with environmental conditions and bacterial activity, Sedimentary Geology, https://doi.org/10.1016/j.sedgeo.2019.04.003

Fe-rich microspheres pseudomorphs after pyrite framboids in Holocene fluvial deposits from NE Spain: relationship with environmental conditions and bacterial activity

María José Mayayo[a*], Alfonso Yuste[a], Aránzazu Luzón[a], Alfonso Corzo[b], Arsenio Muñoz[a], Antonio Pérez[a], Asunción Soriano[a]

[a] IUCA-Departamento de Ciencias de la Tierra, Universidad de Zaragoza, Pedro Cerbuna 12, 50009 Zaragoza, Spain

[b] Departamento de Biología, Facultad de Ciencias del Mar y Ambientales, Universidad de Cádiz, Polígono Río San Pedro, 11510 Puerto Real, Spain

* Corresponding author. E-mail address: mayayo@unizar.es

ABSTRACT

Three iron oxides-rich microsphere types (Type I to III) were detected in an Holocene 17 m-thick stratigraphic succession located in the Iberian Range (NE Spain). Lithofacies features indicate that the studied materials were generated in an alluvial-dominated setting, with a channeled area fringed by floodplain zones. During high water levels and high-energy floods, gravels and sands deposited in the active area and in lateral overbank areas. In these lateral areas, mud settling took place when flood decreased and then anoxic conditions could be reached due to microbial oxidation of organic matter and the low permeability of the marly sediment. X-ray diffraction (XRD) analysis of 32 samples and microtextural observation of 10 samples by Field Emission Scanning Electron Microscopy (FESEM) revealed the occurrence of Fe oxi-hydroxides microspheres showing different surficial structure. These microspheres are pseudomorphs after pyrite framboids although the formation of some primary Fe oxy-hydroxides aggregates cannot be rejected. Pyrite framboids genesis in sediments underlying oxic-dysoxic water column would have been favored by anoxic conditions reached in lateral overbank areas after main flooding, involving the activity of Fe reducing bacteria and sulfate-reducing bacteria (SRB), given the high $SO_4^{=}$ availability provided by the highly mineralized groundwater from the upstream Baños de Ariño spring. Subsequent change to oxic conditions

during the exposition of the floodplain enhanced the transformation of pyrite into Fe oxy-hydroxides, as well as in microenvironments around cracks and roots. Pyrite oxidation likely took place with the implication of neutrophilic iron oxidizing Bacteria and Archaea living in microaerophilic conditions, as well as cyanobacteria, given the close association of Fe oxides framboids with microbial features. In addition, pyrite and/or Fe oxi-hydroxides framboids from marl levels could have been incorporated to sand sediments during further overbank flooding episodes. Under these new oxic conditions pyrite oxidation would have been favored and even the formation of primary Fe oxy-hydroxides.

KEY WORDS: framboids; pyrite; Holocene; alluvial deposits; bacteria

1 INTRODUCTION

Fe-oxides and oxy-hydroxides hematite, goethite, and lepidocrocite, common minerals in natural environments, are frequently used as palaeoenvironmental indicators.

In this paper different types of iron oxides-rich microspheres occurring in an Holocene stratigraphic succession located in the Iberian Range (NE Spain) have been studied. Several authors have identified Fe-oxides spherical aggregates whose formation has been attributed to different processes, with or without bacterial involvement, in various natural environments (Luther III et al., 1982; Merinero et al., 2008; Sgavetti et al., 2009; Bailey et al., 2010; Cavalazzi et al., 2012; Fayek et al., 2012; Potter-McIntyre et al., 2014; Zhang et al., 2014); even within macrofossil remains (Schweitzer and Horner, 1999; Kappler and Newman, 2004; Sawlowicz and Kaye, 2006; Kaye et al., 2008; Blanco et al., 2013). These spherical aggregates have been often interpreted as oxidated pseudomorphs after pyrite framboids.

The formation of pyrite at low ambient temperature (<100^{o} C) is considered to be directly or indirectly linked to the oxidation of organic matter by dissimilatory sulfate reducing bacteria in anoxic conditions (Canfield, 1989; Konhauser, 2007). Pyrite framboids are very common in the geological record and mostly identified in ancient rocks or modern marine anoxic sediments.

However, their occurrence has been scarcely documented in continental deposits and, is restricted to anoxic deep or saline shallow lakes (e.g. Pérez et al., 2002). Conversely, reports of pyrite framboids formation in recent surficial and oxygenated fresh water environments, like the one described here, are very scarce (e.g. Luzón et al., 2011).

The interest on the genesis of iron oxides and hydroxides spherical structures has increased due to recent findings of presence of iron oxides spherules in Mars and their possible relation with photo-oxidation processes of Fe sulfides in aqueous conditions, whose formation has been in some cases related to bacterial activity (Zolotov and Shock, 2005; Sgavetti et al., 2009; Egglestone et al., 2010; Blanco et al., 2013).

Cyanobacterial dominated microbial mats grow frequently on the sediment surface in freshwater, brackish and marine environments subject to frequent oscillation in the water level (Garcia de Lomas et al., 2005, Stal, 2012). This microbial biofilms or mats are complex multispecific community harboring a considerably metabolic diversity. The oxygenic phototrophic community composed by cyanobacteria and other eukaryotic microalgae as well, in the modern microbial mats, provides O_2 and organic matter, which both contribute to support complex heterotrophic and chemolithotrophic communities, which find their ecological niches at different depth within the microbial mats due to the strong gradients of different e^- donors and acceptors (Froelich et al., 1978). In addition microorganisms within the mat are surrounded by an organic matrix of extracellular polymeric substance (EPS) secreted by the microbes themselves (Decho, 2000). The variety of microbial activities, the control of the cycling and exchange of nutrients and other elements at the sediment-water interface, the trapping of sediment particles, and the capacity to bind cations to the negatively charged EPS and cellular surfaces, make the sediment surface in aquatic environments "hot spots" of intense biogeochemical activity, creating the necessary conditions for intense bioweathering and biomineralization (Beveridge et al., 1997; Cuadrado et al., 2012). The role of organic

molecules and polymer matrix is considered essential in regulation of crystal growth, size and their morphology (Mann 1988; Bianconi et al. 1991, Sawlowicz 2000).

The aim of this work is to characterize Fe oxides- and oxy-hydroxides- rich microspheres originated in a fluvial setting during the Holocene and find out the conditions under which they were formed. The present paper documents the probable formation of pyrite framboids at low temperature in an environment where they have been scarcely described, such as fresh water sediments underlying oxic-dysoxic water column. On the other hand, given the characteristics of the materials where the aggregates are found, the palaeoenvironmental conditions under which they were formed, and the different textural types of iron oxide framboids it is considered that the development of these aggregates occurred mainly in flood plain areas with alternating oxic and anoxic conditions in the sediment and through the oxidation of former pyrite framboids. Therefore, the work gives information on the mechanisms of pyrite framboids oxidation to Fe oxides, probably induced by microbial activity. Accordingly, the paper provides insights on the relationship between the variation of the palaeoenvironmental conditions and the processes and mechanisms of pyrite framboids formation and their transformation to Fe oxides.

2 GEOLOGICAL CONTEXT

The study area is located in the medium reaches of the Martín River in the Iberian Range (NE, Spain), downstream of Ariño village (Fig. 1). It is dominated by Mesozoic and Cenozoic rocks involved in E-W to NW-SE trending tectonic structures (folds and thrusts) generated during the alpine orogeny. Mesozoic and Cenozoic units are widely represented in the area. With the exception of the Keuper facies, the Mesozoic units are mainly carbonates. Nevertheless, the siliciclastic Escucha Fm. (Lower Cretaceous) contains thick coal beds and has been mined in the Escuriza River valley, a tributary of the Martín River, since the past century. Cenozoic units are composed of mudstones with interbedded conglomerates. Quaternary deposits, mainly detrital, are commonly associated to the Martín River valley that, in some zones, shows a well-

developed floodplain (Fig. 1). Several Pleistocene and Holocene terrace and glacis levels have been described (Ríos et al., 1981; Lozano et al., 2004; Muñoz et al., 2016; Entrena et al., 2017). The studied samples were collected in "Los Estrechos" area, downstream the Baños de Ariño spring (Fig. 1) and come from a stratigraphic profile (Huerta Perales profile, HP from now) made by Muñoz et al. (2016) in the Holocene "Lower terrace" of Lozano et al. (2004), located 15-20 m over the recent talweg. The studied succession is 17 m-thick (Fig. 2) and mainly horizontal in the profile site, nevertheless far to the river it slightly dips from the valley margins towards the talweg. These deposits represent sedimentation in an alluvial system with the main channel flowing towards the North, as nowadays, that received lateral supplies (Fig. 1). The sedimentary system was fed by surficial waters and also by highly mineralized groundwater (calcic-magnesian sulfate-bicarbonate) from the Baños de Ariño spring, located 3.5 km upstream the sampled profile (Fig. 1). Growth of tufas was locally important (Muñoz et al., 2016; Entrena et al., 2017).

3 METHODS

A detailed log of a stratigraphic profile (HP) was carried out and sedimentary facies defined by their lithology, bed shapes, textural features and sedimentary structures. The chronology of the profile was established by AMS (accelerator mass spectrometry) ^{14}C dating on four charred remain samples. Selection of the samples was conditioned by the presence of organic material trying to avoid potential "hard water effect" problems. Necessary preparation and pre-treatment of samples, as well as radiocarbon dating were carried out in the Centro Nacional de Aceleradores (Sevilla, Spain). ^{14}C ages were calibrated using Calib 7.0 program (Reimer et al., 2013).

The mineralogical composition, whole rock and <2 μm fraction, of 32 samples from the profile under study was determined by X-ray diffraction (XRD) using a Philips PW1710 diffractometer with CuKα radiation, automatic divergence slit and graphite monochromator, from the

University of Zaragoza. The fine fraction was separated by centrifuge and analyzed on air dried and ethylene glycol-treated (at 60 °C for 48 h) oriented aggregates. The XRD data were stored as computer files with the XPowder software (Martín, 2004). To compare the study samples, an estimation of mineral abundance was carried out using the normalized reference intensity ratio method (Chung, 1974; Jenkins and Snyder, 1996) and the weighting factors of Schultz (1964) and Biscaye (1965). The analytical error of the semiquantitative determination is about 5%.

Ten selected samples were analyzed by Field Emission Scanning Electron Microscopy (FESEM) using secondary (SE) and backscattered electron (BSE) images and Energy-Dispersive X-ray (EDS) analysis. The observations were performed using a Carl Zeiss MERLIN FESEM equipped with an Oxford Instruments INCA 350 EDS detector. An accelerating voltage of 4 to 15 kV and a beam current of 1 to 2 nA with a counting time of 50 s were used for analysis. Samples were carbon coated.

4 RESULTS

4.1 Dating and Sedimentary lithofacies

The dating by ^{14}C of four samples from the HP profile (Fig. 2) in the Martín River left bank (Fig. 1) indicated that these materials were deposited in the Holocene (Table 1). Four lithofacies can be recognized in this profile: gravels, sands, marls, and tufas (Table 2). Further information can be found elsewhere (Muñoz et al., 2016).

Gravels (Fig. 3A) are grain-supported, with coarse sand or microconglomerate matrix and carbonate and siliceous rounded-subrounded pebbles and cobbles. They form decimeter-thick, tabular or channeled fining upward bodies with imbrication and trough cross bedding. This lithofacies represents high-energy tractive water flows and deposition in the active fluvial area either in braided channels or in fluvial bars (Hein and Walker, 1977; Miall, 1996). Paleocurrents evince, as nowadays, northwards-directed flows.

Sands are ochre or beige, fine to medium-grained, rarely coarse (Fig. 3B). They form tabular strata 10 to 80 cm-thick, or less frequently channels up to 1.30 m; both are fining upwards. Tabular strata show horizontal and convolute lamination, *climbing ripples* and root traces, and channels through cross bedding. Remains of charred material, tufa and gastropod have been widely recognized. This lithofacies is related to less-energetic tractive flows (Hein and Walker, 1977; Miall, 1996). Two main sites of deposition can be interpreted: i) channels and ii) overbank vegetated areas reached during flooding or channel avulsion episodes. Convolute lamination and *climbing ripples*, suggest high sedimentary rates and rapid deposition (Jopling and Walker, 1968; Allen, 1982).

Marls, sometimes laminated, are predominantly grey, locally brown or ochre (Fig. 3C), and form tabular decimeter-thick beds with up to 5 cm very disperse carbonate clasts. Levels with charred and tufa remains are very common, as well as root traces, which can reach several decimeters in length and 3 cm in diameter, and are usually covered by lenticular gypsum crystals (Fig. 3C). Moreover, gastropods and ostracods are present. This lithofacies evinces mud-settling in episodically flooded, vegetated overbank areas (Miall, 1978; 1996). The existence of tufa and charred remains agrees with such interpretation, being dragged till these areas during flooding events (Luzón et al., 2011). Differences in color indicate changes in soil oxidation conditions, with grey beds related with lower Eh values and ochre ones to more oxic conditions, during which growing of gypsum would took place. Charred remains are mainly related with fires probably generated during dryness episodes.

Tufas form several decimeters-thick phytoherms (boundstone beds) of stems, reeds, and bryophytes (Fig. 3D). Moreover, irregular phytoclastic beds (packstone-rudstone), 10 to 60 cm in thickness, made of fragments up to 2-3 cm with marly matrix, can be identified. This facies represents carbonate precipitation and tufa genesis in overbank areas, river banks, or alternatively, genesis of barriers in the fluvial active zone (Pedley, 1990; Ford and Pedley,

1996); tufa barriers development would have conditioned flooding upstream. Phytoclastic beds reflect tufa erosion during high-energy floods or exposition episodes of the barriers.

4.2 Mineralogical composition

High calcite contents stand out in all the lithofacies (Table 3). Calcite is the main mineral in almost all the samples, except in one case, a gravel level with predominantly siliceous clasts. Sand samples show high quartz contents but also calcite, which, along with their poor or virtually null cementation, points out a mainly detrital origin for calcite. Marl samples show the highest phyllosilicate contents, and tufas, as expected, the highest calcite and the lowest quartz+phyllosilicate contents. Dolomite, gypsum and occasionally feldspars have been detected as minor minerals by XRD. The <2 μm fractions are composed of illite and kaolinite as major minerals, along with mixed-layer illite-smectite as minor phases, and evidences of chlorite in some samples. Illite/kaolinite ratio is close to 2 (1.7). In the <2 μm fraction of five sand samples lepidocrocite (FeOOH) has been identified by XRD. Root traces are covered by lenticular gypsum crystals and filled by phyllosilicates, gypsum, and goethite (hematite is not ruled out although its presence cannot be confirmed).

4.3 Microtextural analysis

FESEM images show that calcite occurs as anhedral crystals of different sizes, which frequently show surface features probably due to dissolution processes (Fig. 4A). Irregular surfaces have been also observed in gypsum (Fig. 4B) and dolomite (Fig. 4C), which could be related to dissolution processes or, as for dolomite, to neoformation of tiny crystals on previous ones. Phyllosilicates occur as micron-sized anhedral particles. Sometimes they appear as larger (up to 40 μm long) aggregates, as in the case of kaolinite (Fig. 4D), probably coming from nearby Cretaceous materials (Utrillas and Escucha Fms.), where kaolinite content doubles illite one

and it frequently occurs as aggregates similar to those described here (González-López et al., 2005).

As above mentioned, in the <2 μm fraction of some sand samples, lepidocrocite (FeOOH) has been identified by XRD. The study of the samples, sands and marls, under the FESEM has showed that Fe-oxides and/or oxi-hydroxides generally occur as loose irregular masses of discrete microcrystalline grains (Fig. 5A) with different morphological features: anhedral nanocrystals (<100 nm) of different sizes (Fig. 5B); skeletal octahedral crystals (≈1 μm) (Fig. 5C); or more or less equidimensional nanocrystals (300-400 nm), some of them probably octahedral, in turn composed of tiny planar crystals arranged face to face (Fig. 5D). In agreement with XRD data, some of these crystals are probably lepidocrocite. In addition, in the sands and marls facies, different sized spherical aggregates of Fe-phases have been frequently identified (Fig. 5E). They usually appear enveloped by a cover that masks their surficial texture (Fig. 5F). Occasionally, microspheres composed of euhedral octahedra have also been observed (Fig. 5G, H) and EDS analyses reveals, in all cases, the presence of O and Fe, and the total lack of S, indicating that the different identified morphologies are exclusively composed of Fe- oxides and/or oxi-hydroxides. Unfortunately, these spherical aggregates could not be separated and concentrated to be analyzed by XRD and thus we are not able to confirm which oxides and/or hydroxides are composed of.

The size of Fe-oxides spherical aggregates varies from 4 to 30 μm, with an average value of 12.4 μm and a mode around 11-12 μm. Three different types of spherical aggregates (Types I, II, and III) have been identified according to the surficial observable structure.

Type I are spherical aggregates composed by equant skeletal crystals (~1 μm). Among these, polygonal sections of polyhedral shapes resembling octahedra can be recognized (Fig. 6A, B). These skeletal crystals are, in turn, composed by nanometric anhedral crystallites randomly arranged.

Type II consist of spherical aggregates made up of subhedral equant crystals with morphologies close to polyhedra and sizes <0.5 μm, composed by planar anhedral nanoparticles arranged face to face (Fig. 6C, D). Backscattered Electron images (BSE) evidence hollow octahedral morphologies (Fig. 6E).

Type I and II aggregates can be described as microscopic spheroidal to sub-spheroidal clusters of equidimensional and equimorphic microcrystals, and subsequently they can be considered as framboids (Ohfuji and Rickard, 2005). Sulfur was not detected by EDS analyses and there is no pyrite evidence by XRD. Nevertheless, skeletal crystals morphologies from Type I framboids point out that these spherical aggregates are the result of Fe-oxides replacement after pyrite framboids constituted by octahedral crystals. In the case of Type II framboids, the presence of occasional skeletal crystals, their morphology and BSE images (Fig. 6E) permit to deduce the same origin proposed for Type I. Type I and II aggregates have been identified in both marls and sands lithofacies.

Type III are spherical aggregates showing an internal structure composed of subspherical morphologies 2-2.5 μm in diameter and covered by acicular or lens-shaped nanocrystals that in some zones appear to have radial distribution (Fig. 6F, G). This can also be observed in BSE images (Fig. 6H). These aggregates could be considered as poliframboids composed of framboids of massive iron oxi-hydroxides after pyrite transformation, developing outer rims, halos and prismatic overgrowth, or "sunflower framboids" (Sawlowicz, 2000; Merinero et al., 2009; 2015) but smaller than those described by these authors. Nevertheless, BSE images show that sometimes the core of the subspheres composing these aggregates have subpolyhedral morphology (Fig. 6H), suggesting that Type III aggregates could also have been pyrite framboids in origin. The surficial textural features of the subspheres constituting these aggregates, covered by radially arranged acicular or lens-shaped nanocrystals, seem to be similar to Fe-oxides botryoidal infills or cements, whose origin would require previous pore

spaces occupied by a solution or a gel. Type III aggregates were identified in this study only in low to unconsolidated, highly porous, ochre or beige sands.

On the other hand, Fe oxides filling root traces show textures similar to Type III aggregates. In this sense, it would appear that Fe oxides constituting Type III aggregates could be goethite, in agreement with XRD data of oxi-hydroxides filling root traces, although it cannot be confirmed with certainty, as commented before.

Interestingly, structures resembling microbial organisms or biological tissue have been observed closely associated to the spherical Fe-oxides aggregates. Some of them consist of nanometrical subspheres arranged in chain-like structures (Fig. 7A); others appear as random clusters of micron-sized ring-shaped structures in close spatial relationship with the spherical aggregates or partially covering them (Fig. 7B). In some cases, the microspheres previously described are nearly covered (Fig. 7C) by a coating of small ellipsoidal capsules (<1 μm), most of them collapsed or perforated (Fig. 7D, E). Cl and Na have been detected by EDS analyses on the latter structures. These elements have not been detected in any other EDS analyses on the samples. Furthermore, a C-rich soft pliable tissue has been observed in the samples (Fig. 7F), sometimes coating the Fe-rich microspheres surface and fitting the crystals (Fig. 5F).

5 DISCUSSION

Lithofacies features evince that the studied materials were generated mainly in an alluvial-dominated setting, with a north-directed main channel area fringed by a floodplain, and lateral alluvial supplies arriving during high-water availability conditions (Fig. 2). Sedimentation and subsequent sediment changes were controlled by fluctuating environmental conditions, mainly by water-level changes due to the cyclical arrival of palaeofloods. The active central area, dominated by braided channels and bars, is represented by the coarser lithofacies (mainly gravels and some sands). Bar growing took place during high-energy floods and high water levels, when wide areas of the valley bottom could be flooded. During these episodes, rapid

sand deposition and dragging of different coarse detrital particles (charred fragments, tufa remains…) took place towards the lateral vegetated overbank areas, where mud settling would dominate when flood decreased and water-level dropped. Differences in color (grey-ochre) indicate changes in the sediment oxidation conditions, with grey and ochre beds related with dominant lower and higher Eh values respectively, and probably flooded vs. emerged floodplain sediments. Many evidences at a macroscopic scale reinforce the interpretation of the frequent changes of environmental conditions in the study area. Charred fragments are likely related with episodic fires during dryness episodes but carried to the fluvial area by subsequent floods. Precipitation of gypsum in relation to root traces is related to a dominated oxic environment. Tufa genesis reflects freshwater conditions and vegetation development that, at least during some stages, grew in overbank areas, channel and bar banks, or alternatively formed barriers in the fluvial active zone that favored flooding upstream during high-water level episodes.

Mineralogical and textural features of the studied materials are, in general, characteristic of detrital origin. Quartz and phyllosilicates are clearly detrital and come from nearby outcropping rocks. Excluding tufas, calcite is mainly detrital too. However, some phases show evidences of authigenesis, such as some highly euhedral dolomite crystals (Fig. 4C). With regard to gypsum, some crystals are probably detrital and show alteration evidences (Fig. 4B) while others are clearly authigenic (Fig. 5E) and partially enclose spherical Fe-oxides aggregates (Fig. 6F). Those covering root traces are obviously authigenic too.

5.1 Type I and II aggregates

As described in the Results section, microtextural features of Type I and II aggregates point out that they are the results of the replacement by Fe oxides of former pyrite framboids. Zhu et al. (2018) have studied the dependence of pyrite oxidation on surface structure and deduced that {111} (octahedra) is the most sensitive facet for pyrite oxidation. Pyrite framboids can be

oxidized and replaced by Fe-oxides-hydroxides over time, leading to a complete loss of sulfur but maintaining the original framboidal structure (Luther III et al.; 1982, Nordstrom, 1982; Suk et al., 1990; Sawlowicz and Kaye, 2006; Soliman and El Goresy, 2012). Fe-oxides observed as loose irregular masses of discrete microcrystalline grains (Fig. 5C) could have been originated after the replacement of euhedral pyrite single crystals as well.

Pyrite framboids are common in the geological record. Their occurrence and genesis have been described in a variety of geological environments (Wilkin et al., 1996; Sawlowicz, 2000; Wilkin and Arthur, 2001; Corzo et al., 2005; Kremer and Kazmierczak, 2005; Merinero et al., 2008; Luzón et al., 2011; Schieber, 2011; Soliman and El Goresy, 2012), and its abiotic synthesis has been more frecuently achieved in laboratory experiments at temperature higher than 60 ^{o}C (Ohfuji and Richard, 2005 and references therein). However, the exact mechanism explaining the formation of pyrite framboids at low temperature is under debate (Konhauser, 2007). Pyrite forms in sedimentary environments from precipitated amorphous iron monosulfide phases (Canfield 1989, Wilkin and Barnes 1997) through a number of different pyritization mechanisms (Konhauser, 2007). Precipitation of FeS occurs in reducing, organic matter-rich environments found in anoxic water columns and in the anoxic layers of sediment when sulfate concentration is high (Wilkin and Barnes 1997, Wilkin and Arthur, 2001). These conditions occur in marine environments or some continental aquatic environments with high sulfate availability like Baños de Ariño spring in this study. In these environments, a large fraction of organic matter is oxidized in anoxic conditions by sulfate reduction (Jørgensen 1982, Canfield 1993, Holmer and Storkholm 2001). Sulfate-reducing bacteria (SRB) oxidizes organic matter with sulfate as final e^- acceptor releasing H_2S to the external medium, although other sulfur compounds (thiosulfate, sulfite and S^o) with intermediate oxidation states can be either used as e^- acceptor or produced as well (Canfield et al., 2005). These conditions favor the formation of pyrite framboids (Berner, 1985). Their high regular organization and the spherical morphology have made several researchers to point to a biogenic origin, suggesting

that framboids are the result of the replacement of former organisms, such as fossilized bacteria, discrete microorganic forms or microbial colonies (Gong et al., 2008). In addition, pyrite framboids tend to form encapsulated within organic tissue and microbial biofilms which likely influence their final morphology (Sawlowicz, 2000).

The number of microcrystals (NM) with an average diameter (d) in a framboid with a diameter (D) can be calculated from the equation $NM = \varphi(D/d)^3$ (Wilkin et al., 1996; Wilkin and Barnes, 1997) where φ is packing coefficient of microcrystals, which is approximately 0.74 (Sloane, 1998) for cubic closed packing. Taking into account the largest and the smallest measured diameter in the studied case, Type I and II framboids would be constituted by approximately 10^3 to 30 x 10^3 crystals, which is the range of NM showed by framboids in modern sediments (Wilkin et al., 1996). Size distribution of pyrite framboids is considered to be an indicator of the environmental conditions under which they were formed (Wilkin et al., 1996; Wignall and Newton, 1998; Wei et al., 2016). Framboids developed under euxinic conditions are generally small, with a narrow size range (4.3 - 6.1 μm), while diagenetic framboids developed in sediments underlying oxic-dysoxic water column are larger (5.7 - 11.9 μm) with a wider size range (Wilkin et al., 1996). Therefore, framboids in the studied sediments, with diameters ranging between 4 and 30 μm and a mean value of 12 μm, could have been formed in sediments underlying oxic-dysoxic water column (Wilkin et al., 1996, Wei et al., 2016). Pyrite framboids formation would require the presence of reactive Fe^{2+} and H_2S, both likely provided by the activity of Fe reducing bacteria and SRB in anoxic conditions (Canfield 1989, Wilkin and Barnes, 1997), being $SO_4^{=}$ availability a limiting factor in fresh water environments (Davidson et al., 1985; Marnette et al., 1993). The size of the nanoparticles constituting the crystals in Type I and Type II framboids, suggests that those particles could be crystal growth subunits or crystal nuclei in the growing crystal surfaces. This is likely due to a high nucleation rate/crystal growth rate ratio, only possible in high to very high supersaturated conditions (Butler and Rickard, 2000; Sawlowicz, 2000). Textural differences between Type I and Type II framboids

could be related to textural differences of the former pyrite framboids and/or to different supersaturation conditions during oxidation.

Taking into account the ideas above, the required conditions for the formation of pyrite framboids were likely reached in marls, with abundant charred remains and plants, as well as root traces, and generated by settling after main flood episodes (Muñoz et al., 2016). Althoug tne Martín River could have supplied detrital pyrite framboids from coal levels from Escucha Fm. (Querol et al., 1989), they were probably formed *in situ* in the studied grey marls.

5.2 Type III aggregates

As suggested in the Results section, Type III aggregates could also have been pyrite framboids in origin, taking into account their textural features.

As stated before, lepidocrocite has been detected in the <2μm fraction of some sand samples where Type III framboids have been observed. Therefore, Type III framboids could be composed of lepidocrocite instead of goethite, as it has been commented before. In this sense, Bower et al (2015) experimentally demonstrated the formation of primary fibrous Fe-Oxi-hydroxides (lepidocrocite and akaganeite) in ilmenite-bearing sands at T between 25 and 37 ^{o}C in the presence of cyanobacterial biofilms. Nevertheles, the studied sands are carbonate-rich and thus very different to the ones studied by Bower et al. (2015). Related to this, Hansel et al. (2005) indicate that in the presence of carbonates there is genesis of goethite rather than of lepidocrocite, which would point out that Type III aggregates would be composed of goethite, in agreement with their textural features similar to those observed in root traces. On the other hand, Hansel et al. (2005) also state that lepidocrocite is favored to form over goethite in the conversion of ferrihydrite in the presence of Cl^{-} at circumneutral pH, wich has been detected by EDS analyses on several Type III aggregates. Thus, although Type III aggregates are very likely composed of goethite after the transformation of previous pyrite framboids, further investigations would be needed to clarify the occurrence of lepidocrocite in

carbonate-rich sands as the studied in this work, and the possibility that these microspheres are primary Fe oxides aggregates.

Taking into account the ideas above, pyrite framboids from underlying marl levels could have been remobilized during palaeofloods and incorporated to sands, where textural features would permit the formation of goethite that probably constitutes Type III framboids. Despite the lack of conclusive data, the presence of cyanobacteria might perhaps permit in some cases the precipitation of lepidocrocite, since cyanobacteria are among the first photosynthetic prokaryotes and frequently dominate the microbial community at the sediment surface in wetlands subjected to intermittent changes in the water level due to their great resistance to desiccation (Garcia de Lomas et al., 2005, Stal, 2012).

5.3 Microbial mediation

Different microbial processes could have played an important role in the formation of the three types of Fe-oxides-hydroxides framboids described in this study. Microorganisms are well known to influence directly or indirectly the formation of both Fe- sulfides and oxi-hydroxides in different natural environments and in laboratory experiments (Ferris et al., 1989; Brown et al., 1999; Kappler and Newman, 2004; Fortin and Langley, 2005; Hegler et al., 2008; Kaye et al., 2008, Toner et al., 2009; Bower et al., 2015).

Type I and very probably Type II framboids were originally formed as pyrite framboids as suggest their textural features, and their presence in carbonaceous matter-rich samples. They are similar to those resulting from replacement of Fe-sulfides by oxides, observed in soft organic tissues within dinosaur bones (Martill and Unwin, 1997; Schweitzer and Horner, 1999; Sawłowicz and Kaye, 2006; Kaye et al., 2008), in different seep environments (Merinero et al., 2008, 2009, Cavalazzi et al., 2012), in ancient organic rich sediments (Soliman and El Goresy, 2012) and in saltmarsh sediments (Luther III et al., 1982). These studies suggested a possible implication of bacterial activity in the formation of the primary pyrite framboids and in its

oxidation and replacement by Fe-oxides. For example, Cavalazzi et al. (2012) have described the occurrence of C-rich filmy, amorphous structures in close relation to Fe-framboids, similar to those observed in the present study, as preserved remnants of bacterial biofilms, suggesting a direct relationship between pyrite framboids formation and microbial activity.

Type III framboids are also probably derived from previous pyrite framboids. The size and shape of the small spheres and ellipsoids covering some Type III framboids (Fig. 7D) are typical features of bacteria and their arrangement and spatial distribution resemble modern bacterial colonies (Toporski et al., 2002). The influence of organic membranes in framboids spherical shape has been already commented (Sawlowicz, 2000).

Moreover, the soft pliable tissues identified in the studied samples (Fig. 5F and 7F) resemble extracellular polymeric substances (EPS) secreted by bacteria to serve them as a protective coating as well as to anchor onto stable surfaces, forming biofilms and microbial mats (Kaye et al., 2008).

Despite that the implication of different groups of microorganisms in the oxidation of pyrite framboids and their replacement by Fe-oxides has been suggested, the possible mechanisms and the potential interplay between biotic and abiotic processes are unknown so far. Cyanobacterial dominated microbial mats grow frequently on the sediment surface in freshwater, brackish and marine environments subject to frequent oscillation in the water level (Garcia de Lomas et al., 2005, Stal, 2012). No evidences of sedimentary structures related to the existence of microbial mats have been observed although they are common in modern environments similar to the studied in this work. It is very probable that they have not been preserved due to the own features of a sedimentary environment as the studied in this work, where detrital material predominates along with recurrent periods of high water levels and high-energy floods.

Acidophilic and neutrophilic iron-oxidizing prokaryotes promotes the oxidation of Fe^{2+} to Fe^{3+} and the precipitation of biogenic iron oxides as extracellular precipitates close to or on the

bacterial cells (Fortin and Langley, 2005; Posth et al., 2014). The implication of acidophilic iron oxidizing bacteria and Archaea in the formation of iron oxides and oxyhidroxides framboids in the depositional paleo-environment of the Martín River bank is unlikely due to the very low pH (< 3) required by these microorganism, which are typically found in environment polluted by acid mine drainage (Baker and Banfield, 2003). However, the ecological niche of neutrophilic iron-oxidizing bacteria which oxidize ferrous iron at circumneutral pH fits better with the possible palaeoenvironment of the Martín River bank. These microorganisms grow in microaerophilic conditions at the oxic-anoxic interface within microbial biolfim or mats that colonize the sediment surface in fresh water, brackish and marine environments. Furthermore, in the anoxic layer of these biofilms, some groups of iron-oxidizing bacteria can oxidize iron using nitrate, perchlorate and chlorate as an e^- acceptor instead of oxygen (Straub et al., 1996, Weber et al., 2006, Posth et al., 2014).

Finally, phototrophic Fe^{2+}-oxidizing bacteria, which are present in modern marine and freshwater environments, can oxidize Fe^{2+} with light as source of energy in anoxic conditions (Kappler and Newman, 2004; Hegler at al., 2008). These microorganisms were present already on early earth and their metabolic activity could contribute to the deposition of banded iron formations in the ancient geological record (Posth et al., 2014; Konhauser et al., 2017). However, the significance of phototrophic Fe^{2+} oxidation processes in the formation of Fe oxides framboids by replacement of previous pyrite framboids is unlike since they can only use dissolved Fe^{2+} but not less soluble Fe^{2+}-minerals such as pyrite (Kappler and Newman, 2004; Hegler at al., 2008). However, phototrophic Fe^{2+}-oxidizing bacteria have been showed to precipitate directly Fe oxides from dissolved Fe^{2+} in cultures (Kappler and Newman, 2004). Those Fe-oxides were constituted by needle- and plate-like particles similar to the observed in Type III framboids (Fig. 6G).

The filaments observed in some samples associated with Fe-oxides Type III framboids (Fig. 7A) are rather interesting because they might represent some type of colonial filamentous cyanobacteria closely attached with Fe-oxides.

In resume, microbial activity could have played an important role in both the formation of precursor pyrite framboids and their transformation to Fe-oxides. The different groups of prokaryotes discussed before can inhabit the sediment-water interface of the sediment in the study palaeoenvironment, constituting microbial biofilm or well-formed thick microbial mats both in the inundated river banks or in lateral ponds left after flooding events. As stated before these microbial mats would have not been preserved as a result of the environment dynamics. The formation of pyrite framboids likely occurred in the deep anoxic layer of such community in close connection with sulfate reduction. The oxidation of pyrite, with the replacement of the framboid structure by iron oxides, likely occurred mainly in periods when the penetration of O_2 within the sediment increased due to a lower water level, root bioturbation, or even to partial erosion of the sediment surface in periods of dryness.

5.4 Environmental implications

The geological and sedimentary setting as well as the environmental conditions during the Holocene in the studied area (Fig. 8) would be favorable for the genesis of the described framboids during early diagenesis, being formed mainly after the oxidation and replacement of previous pyrite framboids.

After main overbank flooding episodes (Fig. 8A), favored by high water availability and damming of water by tufa barriers, anoxic conditions at the sediment-water interface would increase in the floodplain reducing considerably the penetration of oxygen within the sediment. Stagnant non-renewed waters would prevail for a time in these poorly drained areas (Fig. 8B), where the existence of a dense vegetation cover and of cyanobacterial microbial mats in unvegetated areas would supplied organic matter which in turn would support an

intense heterotrophic bacterial activity and consequently a strong consumption of oxygen. These conditions would be more easily reached in non-permeable marl sediments in which water drainage would be impaired. The general increase and extension of the anoxic conditions would lead to an increase of sulfate reduction, providing that there was an available source of sulfate. Surficial waters flowing through the Keuper facies, widely exposed close to the studied profile (Fig. 1), and the spring waters from Baños de Ariño, containing >1300 mg/l $SO_4^{=}$ on average in the last 30 years (Armijo, 2008-2010), likely provided the necessary sulfate to support high rate of sulfate reduction and therefore of H_2S production in this palaeoenvironment. In addition to H_2S, the formation of pyrite framboids requires a source of dissolved Fe^{2+}. Likely, microbial reduction under anoxic conditions of Fe oxides and hydroxides, which are abundant in some levels of the Utrillas Fm. that crops out close to the studied area (Fig. 1), likely provided the necessary soluble Fe^{2+} to support the formation of pyrite framboids (Weber et al. 2006, Kämpf et al., 2012). Taking into account the ideas above, primary pyrite framboids would have formed under the reducing conditions reached in the grey marl sediments under oxic-dysoxic water column, where sulfate reducing Bacteria would have played an important role (Fig. 9A).

Subsequent local or complete exposition of the floodplain would let again to a general increase and extension of oxic conditions in the upper sediment layer and in microenvironments around cracks, roots or animal galleries (Fig. 9A). Redox transition, driven by changes in the oxygen availability, are known to cause wide microbial and biogeochemical effects in the cycling and exchange of different e^- donors and acceptors at the sediment surface (Torres et al., 2014, Corzo et al., 2018). Particularly, the cycling of Fe, between Fe^{2+} and Fe^{3+} and between the aqueous and solid phases, is largely controlled in the natural surface environments by iron oxidizing and iron reducing microorganism, whose activity is determined by the oxygen availability (Weber et al., 2006, Torres et al., 2014, Corzo et al., 2018). Therefore, pyrite framboids could have been oxidized and replaced by iron oxides and hydroxides in marls with

the implication of microorganisms in microaerophilic conditions, given the close association of Fe oxides framboids with microbial features (Fig. 7). The ecological characteristics, likely present in the palaeoenvironment of Martin River bank by comparison with modern analogous, and the microbial features observed in the samples suggest that these microorganisms were likely neutrophilic iron oxidizing Bacteria and Archaea living within a multispecific biofilm or microbial mat (Fig. 9A). Oxidation of pyrite would release $SO_4^{=}$, favoring precipitation of goethite over lepidocrocite (Hansel et al., 2005), as deduced by XRD, and authigenesis of gypsum frequently observed covering root traces. That is to say, Type I and II aggregates observed in marls would have originated through the transformation of previous pyrite framboids under the described conditions with the probable contribution of microbial activity (Fig. 9A).

The described environmental dynamics would make possible that during further overbank flooding episodes (Fig. 8A), pyrite and/or Fe-oxides framboids from underlying marl levels, were remobilized and incorporated to sand deposits (Fig. 9B). In such oxidized environment, pyrite would transform into Fe-oxides as well. Therefore, the environmental dynamics permitted the occurrence of Type I and II framboids in sands. In addition, Type III framboids, which have been only observed in sands and are probably the result of the transformation of previous pyrite framboids, could fit this context as well (Fig. 9B). Nevertheless, Type III aggregates could also represent primary iron oxide framboids precipitated within cyanobacterial dominated microbial mats, which could have been abundant in this palaeoenvironment in some periods of inundations and periodic oscillations in the water level (Fig. 9B) although this point could not be confirmed.

6 CONCLUSIONS

The studied materials were generated in an alluvial setting with a channeled area fringed by floodplain zones. Gravels and sands deposited during high water levels and high-energy floods

in the active area, as well as in lateral overbank areas during flooding. Vegetation and related tufas grew in overbank areas, channel and bar banks, or alternatively formed barriers in the fluvial active zone that favored flooding upstream during high-water level episodes. In lateral overbank areas, mud settling took place when flood decreased. In these areas, anoxic conditions could be reached due to microbial oxidation of organic matter and the low permeability of the marly sediment.

Mineral phases are mainly detrital with the exception of scarce euhedral dolomite crystals and some gypsum, as well as the different occurrences of Fe oxides and/or hydroxides, including loose irregular masses, discrete microcrystals and microspheres. Fe oxy-hydroxides microspheres are pseudomorphs after pyrite framboids although the formation of some primary Fe oxy-hydroxides aggregates is also possible.

In a freshwater, shallow, and broadly oxygenated environment such as that of the current study, pyrite framboids genesis was favored by anoxic conditions reached after main overbank flooding episodes. The oxidation and transformation of pyrite into Fe oxy-hydroxides in marls took place due to a change to oxic conditions during the subsequent exposition of the floodplain and in microenvironments around cracks and roots. Pyrite and/or Fe oxi-hydroxides framboids from marl levels could have been remobilized and incorporated to sands during further overbank flooding episodes. The new oxic conditions would favor former pyrite oxidation and also the formation of primary Fe oxy-hydroxides.

The activity of bacteria, such as sulfate reducing Bacteria (SRB), neutrophilic iron oxidizing Bacteria and Archaea, and cyanobacteria could have been played an important role in the formation and transformation of Fe-rich microspheres.

ACKNOWLEDGEMENTS

This research was funded by the University of Zaragoza (UZ2014-CIE-04, UZ2015-CIE-08). The authors also acknowledge the use of the Servicio de Apoyo a la Investigación–SAI, University of

Zaragoza (Spain). We are very grateful to the reviewer's thorough revision that undoubtedly has helped to improve the manuscript and to *Sedimentary Geology* Editor Brian Jones for revision and editorial handling of the manuscript.

REFERENCES

Allen, J.R.L., 1982. Sedimentary Structures: Their Character and Physical Basis. Elsevier, New York.

Armijo, F., 2008-2010. Historia de los Baños de Ariño a través de sus análisis. Anales de Hidrología Médica 3, 131-158.

Bailey, J. V., Raub T. D., Meckler, A. N., Harrison, B. K., Raub, T. M. D., Green, A. M., Orphan, V. J., 2010. Pseudofossils in relict methane seep carbonates resemble endemic microbial consortia. Palaeogeography, Palaeoclimatology, Palaeoecology 285, 131-142. https://doi.org/10.1016/j.palaeo.2009.11.002.

Baker, B. J., Banfield, J. F., 2003. Microbial communities in acid mine drainage. FEMS Microbiology Ecology 44, 139-152. https://doi.org/10.1016/S0168-6496(03)00028-X.

Berner, R. A., 1985. Sulphate reduction, organic matter decomposition and pyrite formation. Philosophical Transactions of the Royal Society A 315, 25-38. https//doi.org/10.1098/rsta.1985.0027

Beveridge, T. J., Making, S. A., Kadurugamuwa, J. L., 1997. Interactions between biofilms and the environment. FEMS Microbiology Reviews 20, 291-303.

Bianconi, P. A., Lin, J., Strzelecki, A. R., 1991. Crystallization of an inorganic phase controlled by a polymer matrix. Nature 349, 315-317.

Biscaye, P. E., 1965. Mineralogy and sedimentation of recent deep-sea clay in the Atlantic Ocean and adjacent seas and oceans. Geological Society of America Bulletin 76, 803-831.

Blanco, A., Bolaños, U., Lizárraga, L., Hernández, J., Ángeles, S. Ambrocio, S. P., González, M. R., 2013. Microscopic evidences of replacement of iron sulfide by iron oxide in macro fossils:

a useful tool for the search of life in mars? 44th Lunar and Planetary Science Conference (2013). The Woodlands, Texas, pp. 2956.pdf.

Bower, D. M., Hummer, D. R., Steele, A., Kyono, A., 2015. The co-evolution of Fe-oxides, Ti-oxides, and other microbially induced mineral precipitates in sandy sediments: understanding the role of cyanobacteria in weathering and early diagenesis. Journal of Sedimentary Research 85, 1213-1227. https://doi.org/10.2110/jsr.2015.76.

Brown, A. D., Sherriff, B. L., Sawicki, J. A., Sparling, R., 1999. Precipitation of iron minerals by a natural microbial consortium. Geochimica et Cosmochimica Acta 63, 2163-2169. https://doi.org/10.1016/S0016-7037(99)00188-X.

Butler, I. B., Rickard, D., 2000. Framboidal pyrite formation via the oxidation of iron (II) monosulfide by hydrogen sulphide. Geochimica et Cosmochimica Acta 64, 2665-2672. https://doi.org/10.1016/S0016-7037(00)00387-2.

Canfield, D. E., 1989. Reactive iron in marine sediments. Geochimica et Cosmochimica Acta 53, 619-632. https://doi.org/10.1016/0016-7037(89)90005-7.

Canfield, D. E., 1993. Organic matter oxidation in marine sediments. In: Wollast, R., Mackenzie, T., Chou, L. (Eds.), Biogeochemical cycles and global change. Springer, Berlin, Germay, pp. 333-363.

Canfield, D. E., Thamdrup, B., Kristensen, E., 2005. Aquatic Geomicrobiology. Elsevier, Amsterdam.

Cavalazzi, B., Barbieri, R., Cady, S. L., George, A. D., Gennaro, S., Westall, F., Lui, A., Canteri, R., Rossi, A. P., Ori, G. G., Taj-Eddine, K., 2012. Iron-framboids in the hydrocarbon-related Middle Devonian Hollard Mound of the Anti-Atlas mountain range in Morocco: Evidence of potential microbial biosignatures. Sedimentary Geology 263-264, 183-193. https://doi.org/10.1016/j.sedgeo.2011.09.007.

Chung, F. H., 1974. Quantitative Interpretation of X-Ray Diffraction Patterns of Mixtures. II. Matrix-Flushing Method for Quantitative Multicomponent Analysis. Journal of Applied Crystallography 7, 526-531. https://doi.org/10.1107/S0021889874010375.

Corzo, A., Jiménez-Arias, J. L., Torres, E., García-Robledo, E., Lara, M., Papaspyrou, S., 2018. Biogeochemical changes at the sediment–water interface during redox transitions in an acidic reservoir: exchange of protons, acidity and electron donors and acceptors. Biogeochemistry 139, 241-260. https://doi.org/10.1080/01490450500183654.

Corzo, A., Luzón, A., Mayayo, M. J., van Bergeijk, S. A., Mata, P., García de Lomas, J., 2005. Carbonate mineralogy along a biogeochemical gradient in recent lacustrine sediments of Gallocanta Lake (Spain). Geomicrobiology Journal 22, 283-298.

Cuadrado, D. G., Carmona, N. B., Bournod, C. N., 2012. Mineral precipitation on modern siliciclastic tidal flats colonized by microbial mats. Sedimentary Geology 271-272, 58-66. https://doi.org/10.1016/j.sedgeo.2012.06.005.

Davidson, W., Lishman, J. P., Hilton, J., 1985. Formation of pyrite in freshwater sediments: Implications for C/S ratios. Geochimica et Cosmochimica Acta 49, 1615-1620. https://doi.org/10.1016/0016-7037(85)90266-2.

Decho, A.W., 2000. Microbial biofilms in intertidal systems: an overview. Continental Shelf Research 20, 1257-1273. https://doi.org/10.1016/S0278-4343(00)00022-4.

Egglestone, C. M., Parkinson, B. A., Bramlett, E. S., 2010. The hematite-pyrite tandem cell: Avenue to understanding Mars photochemical water oxidation? Goldsmith Conference Abstracts 2010. Knoxville, Tennessee, USA, pp. A261.

Entrena, A., Pérez, A., Muñoz, A., Luzón, A., Mayayo, M. J., Yuste, A., Soriano, M. A., 2017. Morphosedimentary evolution of the Middle Martín Valley (NE Spain) during the Late Pleistocene-Holocene and its relation to climate changes. PAGES-OMS 2017 Abstract Book, Zaragoza, pp. 224.

Fayek, M., Anovitz, L. M., Allard, L. M., Hull, S., 2012. Framboidal iron oxide: Chondrite-like material from the black mat, Murray Springs, Arizona. Earth and Planetary Science Letters 319-320, 251-258. https://doi.org/10.1016/j.epsl.2011.11.033.

Ferris, F. G., Schultze, S., Witten, T. C., Fyfe, W. S., Beveridge, T. J., 1989. Metal Interactions with Microbial Biofilms in Acidic and Neutral pH Environments. Applied and Environmental Microbiology 55, 1249-1257.

Ford, T.D., Pedley, H. M., 1996. A review of tufa and travertine deposits of the world. Earth-Science Reviews 41, 117-175.

Fortin, D., Langley, S., 2005. Formation and occurrence of biogenic iron-rich minerals. Earth-Science Reviews 72, 1-19. https://doi.org/10.1016/j.earscirev.2005.03.002.

Froelich, P. N., Klinkhammer, G. P., Bender, M. L., 1978. Early oxidation of organic matter in pelagic sediments of the eastern equatorial Atlantic: suboxic diagenesis. Geochimica et Cosmochimica Acta 43, 1075-1090. https://doi.org/10.1016/0016-7037(79)90095-4.

García de Lomas, J., Corzo, A., García, C. M., van Bergeijk, S. A., 2005. Microbenthos in a hypersaline tidal lagoon: factors affecting microhabitat community structure and mass exchange at the sediment-water interface. Aquatic Microbial Ecology 38, 53-69.

Gong, Y. M., Shi, G. R., Weldon, E. A., Du, Y., Xu, R., 2008. Pyrite framboids interpreted as microbial colonies within the Permian Zoophycos spreiten from southeastern Australia. Geological Magazine 145, 95-103. https://doi.org/10.1017/S0016756807003974.

Gonzalez, J. M., Bauluz B., Fernandez-Nieto, C., Yuste, A., 2005. Factors controlling the trace-element distribution in fine-grained rocks: the Albian kaolinite-rich deposits of the Oliete Basin (NE Spain). Chemical Geology 214, 1-19. https://doi.org/10.1016/j.chemgeo.2004.08.024.

Hansel, C. M., Benner, S. G., Fendorf, S., 2005. Competing Fe(II)-Induced Mineralization Pathways of Ferrihydrite. Environmental Science & Technology 39, 7147-7153. https://doi.org/10.1021/es050666z.

Hegler, F., Posth, N. R., Jiang, J., Kappler, A., 2008. Physiology of phototrophic iron(II) -oxidizing bacteria: implications for modern and ancient environments. FEMS Microbiology Ecology 66 250-260. https://doi.org/10.1111/j.1574-6941.2008.00592.x.

Hein, F. J., Walker, R. G., 1977. Bar evolution and development of stratification in the gravelly, braided Kicking Horse river, Brithis Columbia. Canadian Journal of Eatrh Sciences 14, 562-570.

Holmer, M., Storkholm, P., 2001. Sulphate reduction and sulphur cycling in lake sediments: a review. Freshwater Biology 46, 431-451. https://doi.org/10.1046/j.1365-2427.2001.00687.x.

Jenkins, R., Snyder, R., 1996. Introduction to X-Ray Powder Diffractometry. Wiley, Hoboken, NJ.

Jopling, A.V., Walker, R. G., 1968. Morphology and origin of ripple-drift cross lamination, whit exemples from the Pleistocene of Massachusets. Journal of Sedimentary Petrology 38, 971-984.

Jørgensen, B. B., 1982. Mineralization of organic matter in the sea bed - The role of sulfate reduction. Nature 296, 643-645.

Kämpf, N., Scheinost, A. C., Schulze, D. G., 2012. Oxide minerals in soils. In: Huang, P. M., Li,Y., Summer, M. E. (Eds.), Handbook of Soil Sciences: Properties and processes. CRC Press, Boca Raton, Fl, pp. 2221-2234.

Kappler, A., Newman, D. K., 2004. Formation of Fe(III)-minerals by Fe(II)-oxidizing photoautotrophic bacteria. Geochimica et Cosmochimica Acta 68, 1217-1226. https://doi.org/10.1016/j.gca.2003.09.006.

Kaye, T. G., Gaugler, G., Sawlowicz, Z., 2008. Dinosaurian Soft Tissues Interpreted as Bacterial Biofilms. PLOS ONE 3 (7), 1-7. https://doi.org/10.1371/journal.pone.0002808.

Konhauser, K. O. (2007). Introduction to geomicrobiology. Blackwell Publishing, Malden, MA.

Konhauser, K. O., Planavsky N. J., Hardisty D. S., Robbins L. J. , Warchola T. J., Haugaard, R., Lalonde, S. V., Partin., C. A., Oonk, P. B. H., Tsikos, H., Lyons, T. W., Bekker, A., Johnson, C. M., 2017. Iron formations: A global record of Neoarchaean to Palaeoproterozoic environmental history. Earth-Science Reviews 172, 140-177. https://doi.org/10.1016/j.earscirev.2017.06.012.

Kremer, B., Kazmierczak, J., 2005. Cyanobacterial mats from silurian black radiolarian cherts: phototrophic life at the edge of darkness? Journal of Sedimentary Research 75, 897-906. https://doi.org/10.2110/jsr.2005.069.

Lozano, M. V., Peña, J. L., Longares, L. A., Sánchez, M., 2004. Cañones del río Martín entre Oliete y Albalate del Arzobispo (Cordillera Ibérica, Teruel). In: Peña,J. L., Longares, L. A., Sánchez, M. (Eds.), Geografía Física de Aragón. Aspectos generales y temáticos. Universidad de Zaragoza e Institución Fernando el Católico, Zaragoza, España, pp. 214-230.

Luther III, G. W., Giblin, A., Howarth, R. W., Ryans R. A., 1982. Pyrite and oxidized iron mineral phases formed from pyrite oxidation in salt marsh and estuarine sediments. Geochimica et Cosmochimica Acta 46, 2665-2669. https://doi.org/10.1016/0016-7037(82)90385-4.

Luzón, M. A., Pérez, A., Borrego, A. G., Mayayo, M. J., Soria, A. R., 2011. Interrelated continental sedimentary environments in the central Iberian Range (Spain): Facies characterization and main palaeoenvironmental changes during the Holocene. Sedimentary Geology 239, 87-103. https://doi.org/10.1016/j.sedgeo.2011.06.005.

Mann, S., 1988. Molecular recognition in biomineralization. Nature 332, 119-124.

Marnette, E. C. L., Van Breemen, N., Hordjik, K. A., Cappenberg, T. E., 1993. Pyrite formation in two freshwater systems in the Netherlads. Geochimica et Cosmochimica Acta 57, 4165-4177. https://doi.org/10.1016/0016-7037(93)90313-L.

Martill, D. M., Unwin, D. M., 1997. Small Spheres in Fossil Bones: Blood Corpuscles or Diagenetic Products? Palaeontology 40, 619–624.

Martín, J. D., 2004. Using XPowder: A Software Package for Powder X-Ray Diffraction Analysis. Retrieved 18 April 2007 from www.xpowder.com. ISBN: 84-609-1497-6.

Merinero, R., Lunar R., Martínez-Frías, J., Somoza, L., Díaz-del-Río, V., 2008. Iron oxyhydroxide and sulphide mineralization in hydrocarbon seep-related carbonate submarine chimneys, Gulf of Cadiz (SW Iberian Peninsula). Marine and Petroleum Geology 25, 706-713.

Merinero, R., Lunar, R., Cardenes, V., Somoza L., González, F. J., 2015. Sunflower micro-pyrite in methane-derived carbonate pipes of the Gulf of Cadiz. Resúmenes sobre el VIII Simposio MIA15, Málaga, Spain, pp. 165-168.

Merinero, R., Lunar, R., Somoza, L., Díaz-Del-Río, V., Martínez-Frías, J., 2009. Nucleation, growth and oxidation of framboidal pyrite associated with hydrocarbon-derived submarine chimneys: lessons learned from the gulf of Cadiz. European Journal of Mineralogy 21, 947-961. https://doi.org/10.1127/0935-1221/2009/0021-1956.

Miall, A. D., 1978. Lithofacies types and vertical profile models in braided river deposits: a summary. In: Miall, A. D. (Ed.), Fluvial Sedimentology. Canadian Society of Petroleum Geologists Memoir 5, pp. 597-604.

Miall, A. D., 1996. The geology of fluvial deposits. Sedimentary Facies, Basin Analysis, and Petroleum Geology. Springer-Verlag, Berlin, Heidelberg.

Muñoz, A., Pérez, A., Mayayo, M. J., Luzón, A., Yuste, A., Soriano, M. A., 2016. Estudio sedimentológico y mineralógico de los depósitos aluviales y fluviolacustres holocenos de los Baños de Ariño. (Cordillera Ibérica, NE de España). Geo-Temas 16, 229-232.

Nordstrom, D. K. (1982). Aqueous pyrite oxidation and the consequent formation of secondary iron minerals. In: Kittrick, J. A., Fanning, D. S., Hossner, L. R. (Eds.), Acid Sulfate Weathering. Soil Science Society of America Special Publication 10, Madison, pp. 37-56.

Ohfuji, H., Rickard, D., 2005. Experimental syntheses of framboids—a review. Earth Science Reviews 71, 147-170. https://doi.org/10.1016/j.earscirev.2005.02.001.

Pedley, H. M., 1990. Classification and environmental models of cool freshwater tufas. Sedimentary Geology 68, 143-154.

Pérez, A., Luzón, A., Roc, A. C., Soria, A. R., Mayayo, M. J., Sánchez, J. A., 2002. Sedimentary facies distribution and genesis of a recent carbonate-rich saline lake: Gallocanta Lake, Iberian Chain, NE Spain. Sedimentary Geology 148, 185-202. https://doi.org/10.1016/S0037-0738(01)00217-2.

Posth, N. R., Canfield, D. E., Kappler, A., 2014. Biogenic Fe(III) minerals: from formation to diagenesis and preservation in the rock record. Earth Sciences Reviews 135, 103-121. https://doi.org/10.1016/j.earscirev.2014.03.012.

Potter-McIntyre S. L., Chan, M. A., McPherson, B. J., 2014. Textural and Mineralogical Characteristics of Microbial Fossils Associated with Modern and Ancient Iron (Oxyhydr) Oxides: Terrestrial Analogue for Sediments in Gale Crater. Astrobiology 14, 1-14. https://doi.org/10.1089/ast.2013.0974.

Querol, X., Chinchón, J. S., López, A., 1989. Distribución del azufre en los carbones albienses de la cuenca del Maestrazgo. Acta Geológica Hispánica 1, 21-32.

Reimer, P. J., Bard, E., Bayliss, A., Beck, J. W., Blackwell, P. G., Bronk Ramsey, C., Buck, C. E., Cheng, H., Edwards, R. L., Friedrich, M., Grootes, P. M., Guilderson, T. P., Haflidason, H., Hajdas, I., Hatté, C., Heaton, T. J., Hoffmann, D. L., Hogg, A. G., Hughen, K. A., Kaiser, K. F., Kromer, B., Manning, S. W., Niu, M., Reimer, R. W., Richards, D. A., Scott, E. M., Southon, J. R., Staff, R. A., Turney, C. S. M., van der Plicht, J., 2013. IntCal13 and Marine13 Radiocarbon Age Calibration Curves 0–50,000 Years cal BP. Radiocarbon 55, 1869–1887. https://doi.org/10.2458/azu_js_rc.55.16947.

Ríos, L. M., Beltrán, F. J., Lanaja, J. M., Martín, F. M., 1980. Cartografía geológica y memoria explicativa. In: Barnolas, A. (Ed.), Mapa Geológico de España 1:50.000, Hoja n° 467 (Muniesa). Instituto Geológico y Minero de España, Madrid.

Sawlowicz, Z., 2000. Framboids: from their origin to application. Prace Mineralogiczne 88, 1-80.

Sawłowicz, Z., Kaye, T. G., 2006. Replacement of iron sulphides by oxides in the dinosaur bone from the Lance Fm. (Wyoming, USA)–preliminary study. Mineralogia Polonica Special Papers 29, 184-187.

Schieber, J., 2011. Iron Sulfide formation. In: Reitner, J., Thiel, V. (Eds.), Encyclopedia of geobiology. Springer Verlag, Berlin, pp. 486-502.

Schultz, L. G., 1964. Quantitative interpretation of mineralogical composition from X-ray and chemical data for Pierre shale. US Geological Survey Professional Paper 391-c, pp 31. https://doi.org/10.3133/pp391C.

Schweitzer, M.H., Horner, J. R., 1999. Intravascular microstructures in trabecular bone tissues of Tyrannosaurus rex. Annales de Paleontologie 85, 179-192. https://doi.org/10.1016/S0753-3969(99)80013-5.

Sgavetti, M., Pompilio, L., Roveri, M., Manzi, V., Valentino G. M., Lugli, S., Carli, C., Amici, S., Marchese, F., Lacava, T., 2009. Two geologic systems providing terrestrial analogues for the exploration of sulfate deposits on Mars: Initial spectral characterization. Planetary and Space Science 57, 614-627. https://doi.org/10.1016/j.pss.2008.05.010.

Sloane, N. A., 1998. Kepler's conjecture confirmed. Nature 395, 435-436.

Soliman, M. F., El Goresy, A., 2012. Framboidal and idiomorphic pyrite in the upper Maastrichtian sedimentary rocks at Gabal Oweina, Nile Valley, Egypt: Formation processes, oxidation products and genetic implications to the origin of framboidal pyrite. Geochimica et Cosmochimica Acta 90, 195-220. https://doi.org/10.1016/j.gca.2012.05.004.

Stal, L. J., 2012. Cyanobacterial mats and stromatolites. In: Whitton, B. A. (Ed.), Ecology of Cyanobacteria II: Their Diversity in Space and Time. Springer, Dordrecht, pp. 65-126. https://doi.org/10.1007/978-94-007-3855-3_4

Straub, K. L., Benz, M., Schink, B., Widdel, F., 1996. Anaerobic, nitrate-dependent microbial oxidation of ferrous iron. Applied and Environmental Microbiology 62, 1458-1460.

Suk, D., Peacor, D. R., Van Der Voo, R., 1990. Replacement of pyrite framboids by magnetite in limestone and implications for paleo-magnetism. Nature 345, 611-613.

Toner, B. M., Santelli, C., Marcus M. A., Wirth, R., Chan C. S., McCollom, Th., Bach, W., Edwards, K. J., 2009. Biogenic iron oxyhydroxide formation at mid-ocean ridge hydrothermal vents: Juan de Fuca Ridge. Geochimica et Cosmochimica Acta 73, 388-403. https://doi.org/10.1016/j.gca.2008.09.035.

Toporski, J., Steele, A., Westall, F., Avci, R., Martill, D. M., Mckay, D.S., 2002. Morphologic and spectral investigations of exceptionally well-preserved bacterial biofilms from the Oligocene Enspel Formation, Germany. Geochimica et Cosmochimica Acta 66, 1773-1791. https://doi.org/10.1016/S0016-7037(01)00870-5.

Torres, E., Ayora, C., Jiménez-Arias, J. L., 2014. Benthic metal fluxes and sediment diagenesis in a water reservoir affected by acid mine drainage: a laboratory experiment and reactive transport modeling. Geochimica et Cosmochimica Acta 139, 344-361. https://doi.org/10.1016/j.gca.2014.04.013.

Weber, K. A., Achenbach, L. A., Coates J. D., 2006. Microorganisms pumping iron: Anaerobic microbial iron oxidation and reduction. Nature Reviews Microbiology 4, 752-764. https://doi.org/10.1038/nrmicro1490.

Wei, H., Wei, X., Qiuc, Z., Song, H., Shi, G., 2016. Redox conditions across the G–L boundary in South China: Evidence from pyrite morphology and sulfur isotopic compositions. Chemical Geology 440, 1-14. https://doi.org/10.1016/j.chemgeo.2016.07.009.

Wignall, P. B., Newton, R., 1998. Pyrite framboid diameter as a measure of oxygen deficiency in ancient mudrocks. American Journal of Science 298, 537-552. https://doi.org/10.2475/ajs.298.7.537

Wilkin, R. T., Arthur, M. A., 2001. Variations in pyrite texture, sulfur isotope composition, and iron systematics in the Black Sea: evidence for Late Pleistocene to Holocene excursions of

the O_2-H_2S redox transition. Geochimica et Cosmochimica Acta 65, 1399-1416. https://doi.org/10.1016/S0016-7037(01)00552-X.

Wilkin, R. T., Barnes, H. L., 1997. Formation processes of framboidal pyrite. Geochimica et Cosmochimica Acta 61, 323-339. https://doi.org/10.1016/S0016-7037(96)00320-1.

Wilkin, R. T., Barnes, H. L., Brantley, S. L. (1996). The size distribution of framboidal pyrite in modern sediments: An indicator of redox conditions. Geochimica et Cosmochimica Acta 60**,** 3897-3912. https://doi.org/10.1016/0016-7037(96)00209-8.

Zhang, H., Shen, H., Cao, C. H., Zheng, Q., 2014. Origins of microspherules from the Permian–Triassic boundary event layers in South China. Lithos 204, 246-257. https://doi.org/10.1016/j.lithos.2014.02.018.

Zhu, J., Xian, H., Lin, X., Tang, H., Dua, R., Yang, Y., Zhu, R., Liang, X., Wei, J., Teng, H. H., He, H., 2018. Surface structure-dependent pyrite oxidation in relatively dry and moist air: Implications for the reaction mechanism and sulfur evolution. Geochimica et Cosmochimica Acta 228, 259-274. https://doi.org/10.1016/j.gca.2018.02.050.

Zolotov, M. Y., Shock, E. L., 2005. Formation of jarosite-bearing deposits through aqueous oxidation of pyrite at Meridiani Planum, Mars. Geophysical Research Letters 32, L21203. https://doi.org/10.1029/2005GL024253.

ACKNOWLEDGEMENTS

This research was funded by the University of Zaragoza (UZ2014-CIE-04, UZ2015-CIE-08). The authors also acknowledge the use of the Servicio de Apoyo a la Investigación–SAI, University of Zaragoza (Spain). We are very grateful to the reviewer's thorough revision that undoubtedly has helped to improve the manuscript and to *Sedimentary Geology* Editor Brian Jones for revision and editorial handling of the manuscript.

TABLES AND FIGURE LEGENDS

FIGURE 1. Geological map of the study area (modified from Rios et al., 1980) in NE Spain. A star indicates location of the stratigraphic profile from which the analyzed samples come from.

FIGURE 2. Huerta Perales stratigraphic profile showing the sedimentary facies and ^{14}C cal ages. Samples position (labelled HP-1 to HP-32), their mineralogical composition and %ill/Kln have also been included. Colored sample labels correspond to those observed under FESEM, stars indicating the presence of microspheres.

FIGURE 3. Close view of some of the sedimentary facies recognised in HP profile. (A) Gravels intercalated in bioturbated marls. (B) Horizontal and cross laminated sands. (C) Marls with root traces covered by lenticular gypsum crystals. (D) Tufas; stem phytoherms.

FIGURE 4. FESEM images of textural features of several minerals observed in the studied samples. (A) Anhedral calcite crystals of different sizes showing surface features probably due to dissolution processes. (B) Gypsum crystal with irregular surfaces, which could be related to dissolution processes. (C) Dolomite crystal with irregular surfaces. (D) Kaolinite aggregate up to 40 μm long. Cal: calcite; Gp: gypsum; Dol: dolomite; Kln: kaolinite.

FIGURE 5. FESEM images showing Fe-oxides and/or oxi-hydroxides with different morphological features. (A) Loose irregular masses of discrete microcrystalline grains embedded in undifferentiated phyllosilicates. (B) Anhedral nanocrystals (<100 nm) of Fe-oxides and/or oxi-hydroxides. (C) Skeletal octahedral crystals (≈1 μm). (D) Equidimensional nanocrystals (300-400 nm) composed of tiny planar crystals arranged face to face. (E) Different sized spherical aggregates of Fe-phases identified in sands and marls. (F) Spherical aggregate of Fe-oxides and/or oxi-hydroxides enveloped by a cover that masks its surficial texture. (G) Microsphere composed of euhedral octahedra. (H) Close view of the euhedral octahedra showed in (G). Fe Ox: iron oxi/oxi-hydroxides; Cal: calcite; Gp: gypsum.

FIGURE 6. FESEM images of spherical aggregates. (A) Type I spherical aggregate; a close view of the area within the white rectangle is showed in (B). (B) Close view of equant skeletal

crystals (~ 1 μm) with polygonal sections of polyhedral shapes resembling octahedra composed by nanometric anhedral crystallites randomly arranged. (C) Type II spherical aggregate; the white rectangle corresponds to (D). (D) Subhedral equant crystals with morphologies close to polyhedra and sizes <0.5 μm, composed by planar anhedral nanoparticles arranged face to face. (E) Backscattered Electron image (BSE) of Type II aggregate evidence hollow octahedral morphologies. (F) Type III spherical aggregate; the white rectangles correspond to figures 7A and B. (G) Type III aggregate internal structures composed of subspherical morphologies 2-2.5 μm in diameter covered by acicular or lens-shaped nanocrystals. (H) BSE image of the internal structure of a Type III aggregate. Fe Ox: iron oxi/oxi-hydroxides; Gp: gypsum.

FIGURE 7. (A) Close view of figure 6F showing nanometrical subspherical structures forming chains that can be observed in a Type III spherical aggregate. (B) Close view of figure 6F: random clusters of micron-sized ring-shaped structures in close spatial relationship with a Type III spherical aggregate that partially cover it. (C) Spherical aggregate covered by organic structures; white rectangles correspond to (D) and (E). (D) Close view of the small ellipsoidal capsules (<1 μm) covering a Type III spherical aggregate. (E) Organic structures collapsed or perforated and EDS analysis showing Cl and Na contents; arrow points to the precise spot for EDS analysis. (F) C-rich soft pliable tissue sometimes coating the Fe-rich microspheres surface and fitting the crystals. Fe Ox: iron oxi/oxi-hydroxides; Qtz: quartz; Phy: phyllosilicates.

FIGURE 8. Sedimentological models showing the two opposite palaeoenvironmental situations, and related sedimentation features, inferred for the Martín River valley during the Holocene. (A) During high water level stages high energy floods reworked sediments previously deposited in channels and floodplains. Lenticular levels evince channel sedimentation whereas lateral tabular, fine sand-mud levels represent overbank deposits. Fining-upwards cycles are related to decreasing water energy conditions after flooding. (B)

After main flooding episodes water level dropped, floodplains remained exposed and vegetation growing was favored. During these stages, fresh water ponds could have been developed in poorly drained areas, whereas gypsum crystals represent high concentrated waters probably in relation with dry environmental conditions.

FIGURE 9. Sedimentary environment and environmental conditions that would be favorable for framboids formation and oxidation during sedimentation and early diagenesis. (A) After overbank flooding episodes, primary pyrite framboids would have formed in the grey marl sediments under oxic-dysoxic water column, where anoxic conditions were reached; sulfate reducing Bacteria would have played an important role in the formation of primary pyrite framboids. Subsequent local or complete exposition of the floodplain would let to a general increase and extension of oxic conditions in the upper sediment layer and in microenvironments around cracks, roots or animal galleries, favoring the transformation of previous pyrite framboids into Types I and II aggregates, with the probable contribution of iron oxidizing Bacteria and Archaea activity. (B) Further overbank flooding episodes would make possible that pyrite and/or Fe-oxides framboids from underlying marl levels, were remobilized and incorporated to sand deposits, where pyrite would transform into Fe-oxides (Types I, II and III framboids) given such an oxidized environment along with the probable involvement of organisms activity, such as iron oxidizing Bacteria and Archaea. The possibility of primary iron oxide framboids formation (Type III aggregates) within cyanobacterial dominated microbial mats in the sands cannot be discarded and remains uncertain.

TABLE 1. AMS radiocarbon dates on organic matter. AMS ^{14}C measurements were calibrated using Calib 7.0.

Sample	^{14}C cal age (yr BP)	Calibrated age 2σ (95%) Cal. BP
HP-11	8728 ± 38	9722 ± 166
HP-17	9508 ± 41	10842 ± 234
HP-26	6363 ± 35	7300 ± 118
HP-28	7576 ± 37	8384 ± 44

TABLE 2. Main features and interpretation of the sedimentary facies identified in Huerta Perales stratigraphic profile as well as in other nearby sections.

Facies		Sedimentological features	Interpretation
Gravels		Grain-supported gravels with sand matrix. Rounded-subrounded clasts, 5 to 15 cm in diameter. Finning upwards tabular or channelled bodies up to 2 m in thickness with imbrication and cross bedding.	Braided channels and longitudinal bars High-energy tractive water flows **Axial Fluvial System**
Sands		Fine to medium-size sands in tabular, sometimes channelled, strata (10 to 130 cm-thick). Tabular strata can include parallel and cross lamination as well as ripples and root traces. Channels are finning-upwards and show cross bedding. Coal and tufa debris are common.	Overbank or channel deposits **Low-energy water flows mainly related to the Axial Fluvial System**
Marls		Brown or grey, sometimes laminated, carbonate mud in tabular, 10 to 1,4 cm-thick, strata. Common coal debris and root traces. Brown levels include limestone clasts and grey ones tufa debris and rare gastropod and ostracods remains.	Mud settling in vegetated floodplains with coarse supplies during high-energy flooding. **Axial Fluvial System and Lateral Alluvial Fans**
Tufas	**Phytoherms**	Carbonate-encrusted stems, reeds and bryophytes.	Carbonate precipitation and tufa genesis **Marginal River Areas or Barriers**
	Rudstones	Irregular beds, 10 to 60 cm in thickness, made on tufa phytoclasts with marl matrix.	Tufa erosion due to high-energy floods or exposition **Axial Fluvial System**

TABLE 3. Mean mineralogical composition and ranges (XRD) of the four lithofacies recognized in HP profile. Calcite, Cal; quartz, Qtz; feldspards, Fsp; phyllosilicates, Phy; dolomite, Dol; and gypsum, Gp.

		Cal (%)	Qtz (%)	Fsp (%)	Phy (%)	Dol (%)	Gp (%)
GRAVELS	mean	23	65	0	10	<5	0
SANDS	mean	44	32	<5	17	<5	<5
	range	30-64	9-44	0-<5	9-26	<5-7	0-5
MARLS	mean	45	22	<5	28	<5	<5
	range	26-76	6-40	0-<5	17-44	0-6	0-<5
TUFAS	mean	64	11	0	24	<5	<5
	range	47-82	<5-22	0-0	16-33	0-5	0-<5

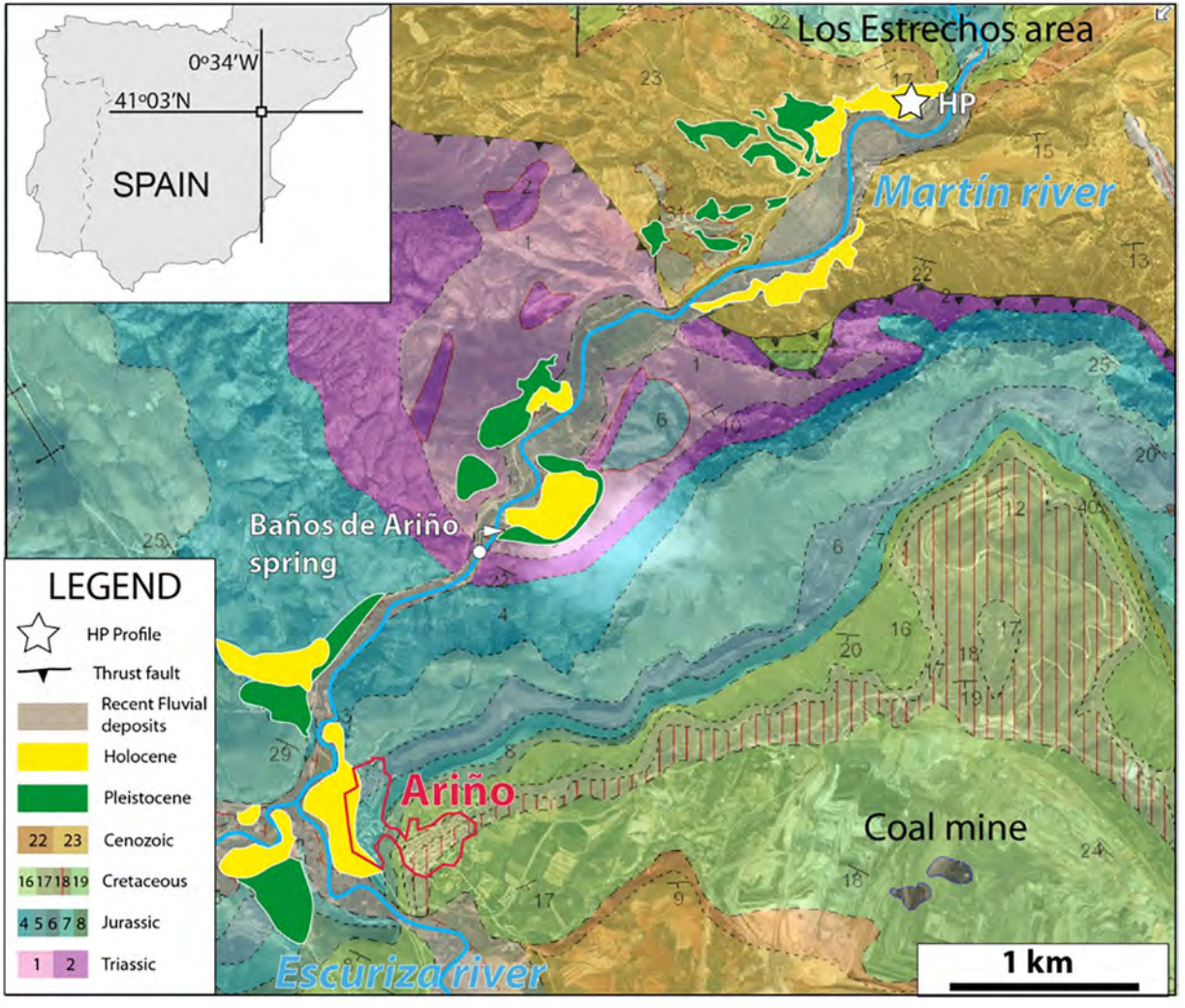
0°34'W
41°03'N
SPAIN
Los Estrechos area
HP
Martín river
Baños de Ariño spring
Ariño
Coal mine
Escuriza river
1 km
LEGEND
HP Profile
Thrust fault
Recent Fluvial deposits
Holocene
Pleistocene
22 23 Cenozoic
16 17 18 19 Cretaceous
4 5 6 7 8 Jurassic
1 2 Triassic

Figure 1

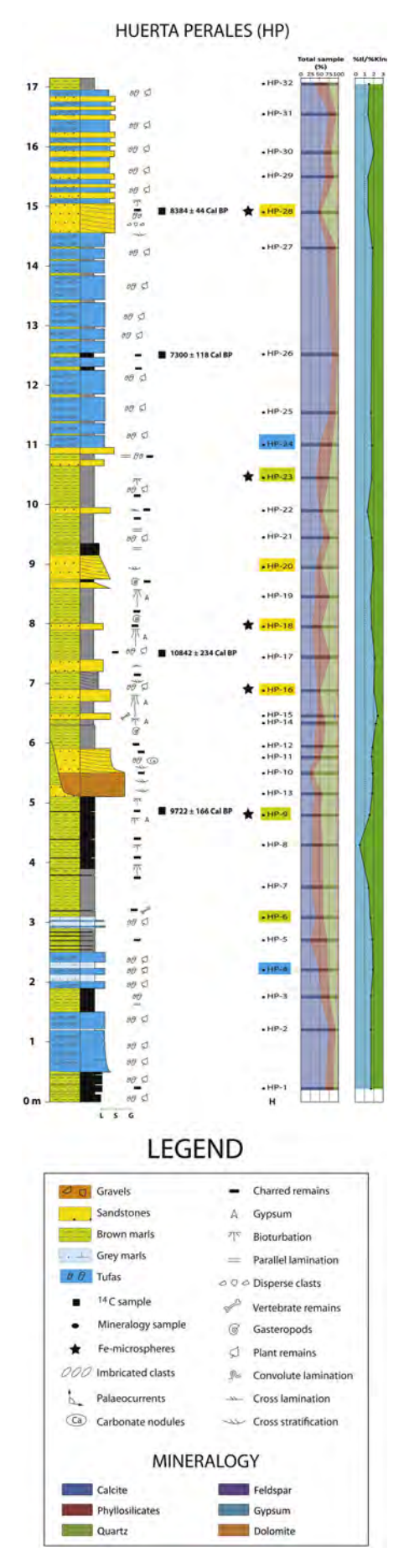
HUERTA PERALES (HP)
Total sample (%)
0 25 50 75 100
%I/%Kln
0 1 2 3
17
16
15
14
13
12
11
10
9
8
7
6
5
4
3
2
1
0 m
8384 ± 44 Cal BP
7300 ± 118 Cal BP
10842 ± 234 Cal BP
9722 ± 166 Cal BP
HP-32
HP-31
HP-30
HP-29
HP-28
HP-27
HP-26
HP-25
HP-24
HP-23
HP-22
HP-21
HP-20
HP-19
HP-18
HP-17
HP-16
HP-15
HP-14
HP-12
HP-11
HP-10
HP-13
HP-9
HP-8
HP-7
HP-6
HP-5
HP-4
HP-3
HP-2
HP-1
L S G
H
LEGEND
Gravels
Sandstones
Brown marls
Grey marls
Tufas
14C sample
Mineralogy sample
Fe-microspheres
Imbricated clasts
Palaeocurrents
Carbonate nodules
Charred remains
Gypsum
Bioturbation
Parallel lamination
Disperse clasts
Vertebrate remains
Gasteropods
Plant remains
Convolute lamination
Cross lamination
Cross stratification
MINERALOGY
Calcite
Phyllosilicates
Quartz
Feldspar
Gypsum
Dolomite

Figure 2

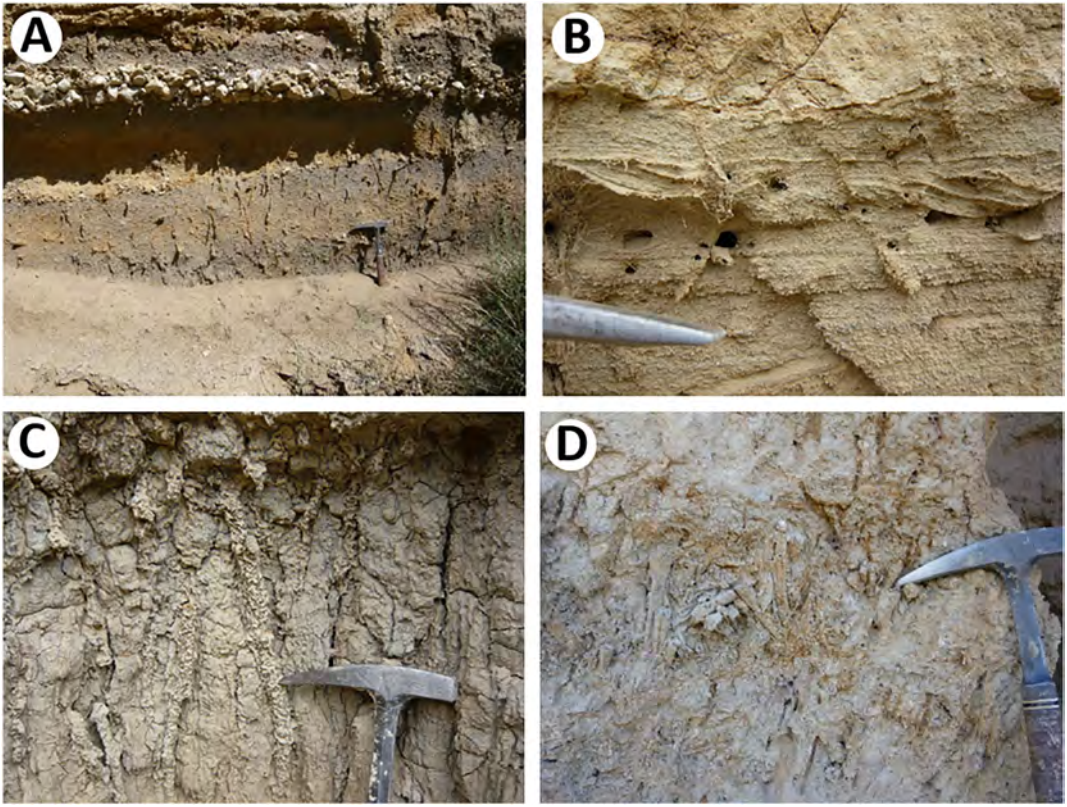

Figure 3

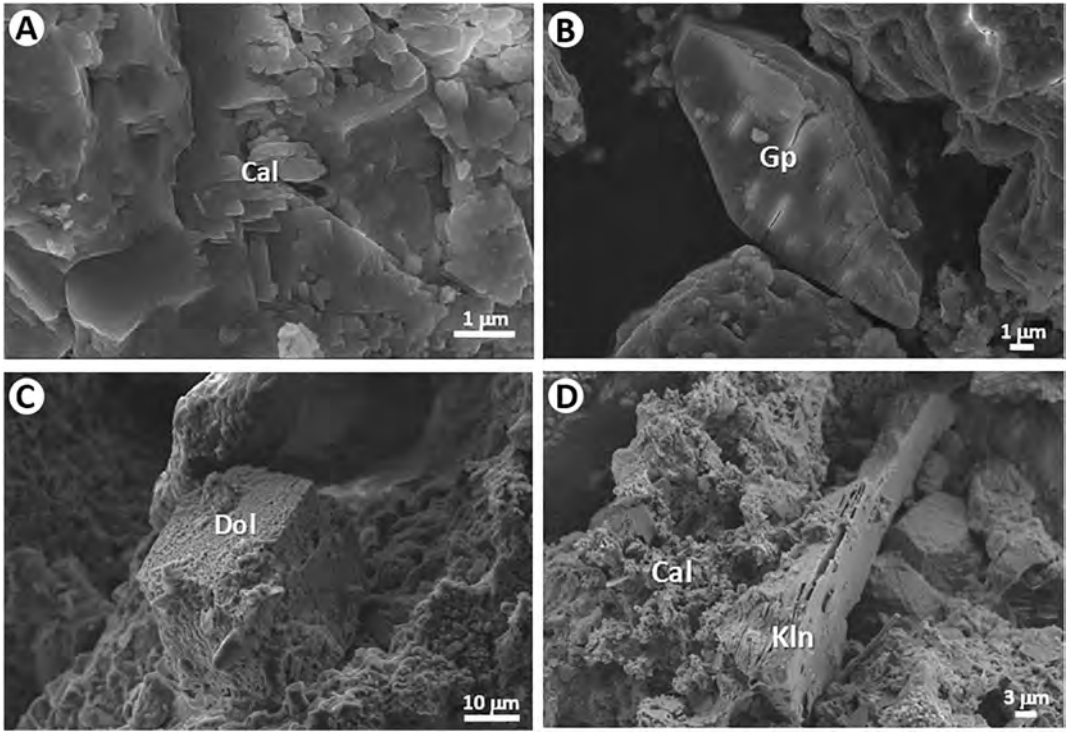

Figure 4

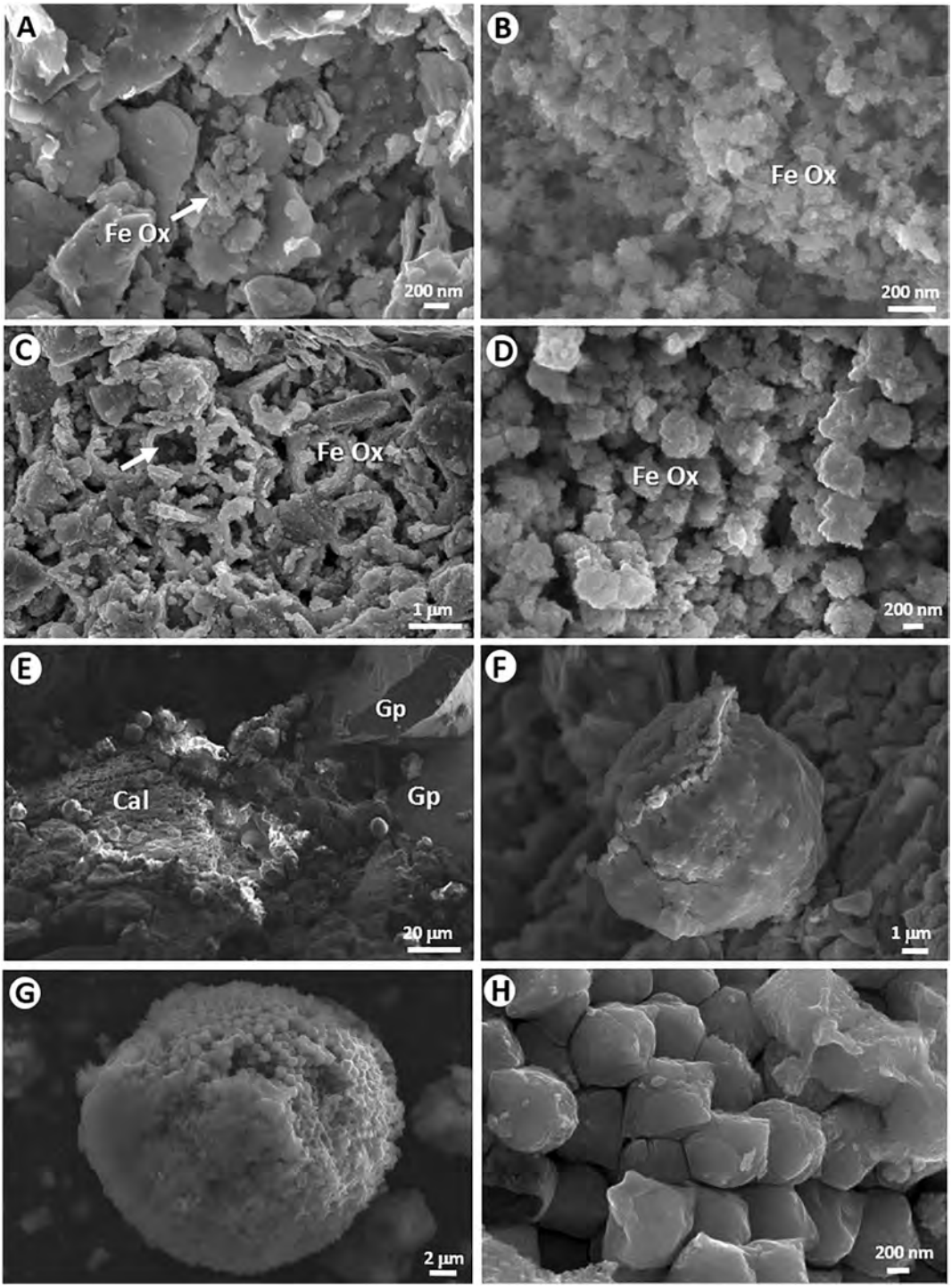
A
Fe Ox
200 nm
B
Fe Ox
200 nm
C
Fe Ox
1 µm
D
Fe Ox
200 nm
E
Gp
Cal
Gp
20 µm
F
1 µm
G
2 µm
H
200 nm

Figure 5

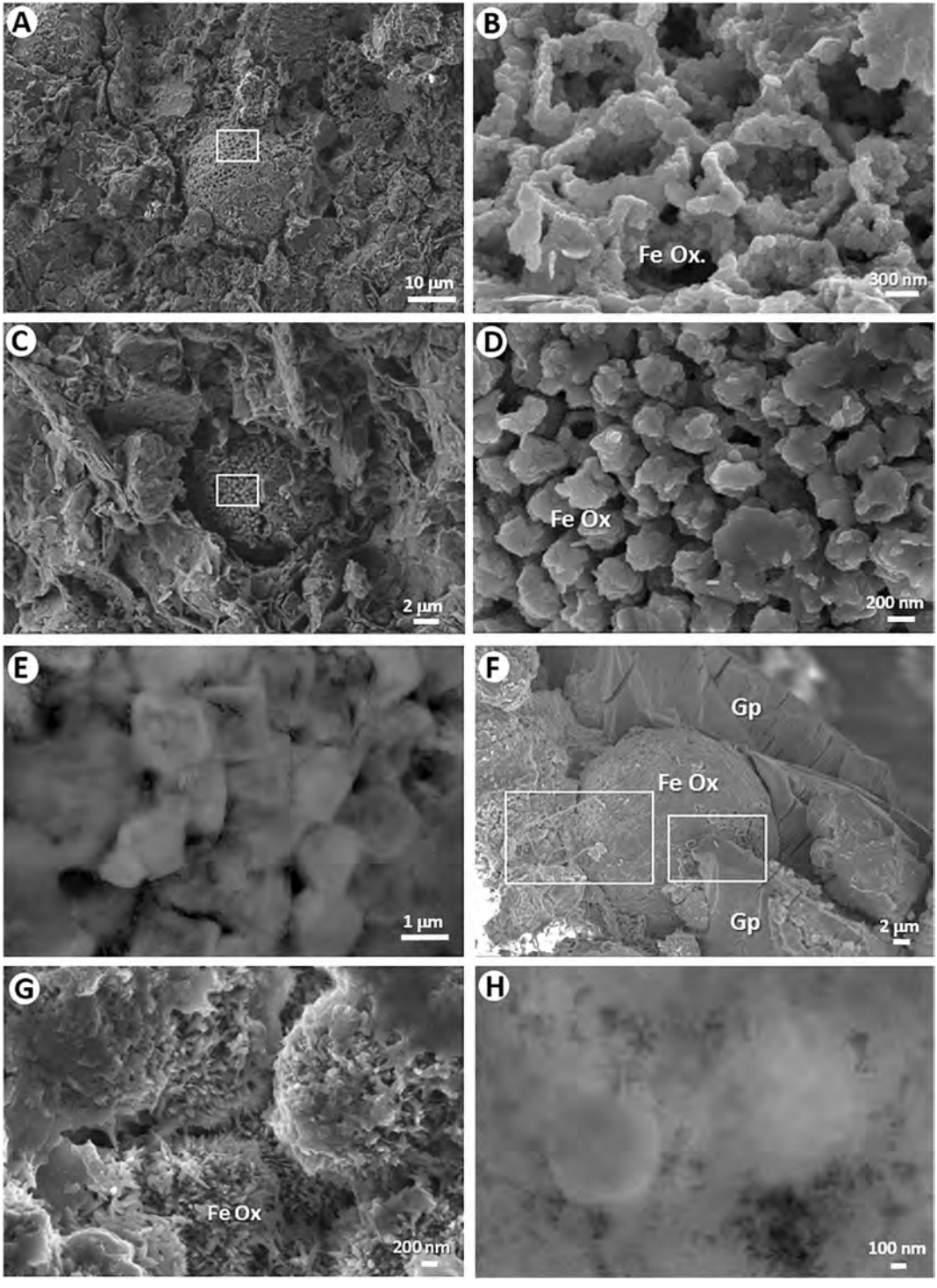
A
10 µm
B
Fe Ox.
300 nm
C
2 µm
D
Fe Ox
200 nm
E
1 µm
F
Gp
Fe Ox
Gp
2 µm
G
Fe Ox
200 nm
H
100 nm

Figure 6

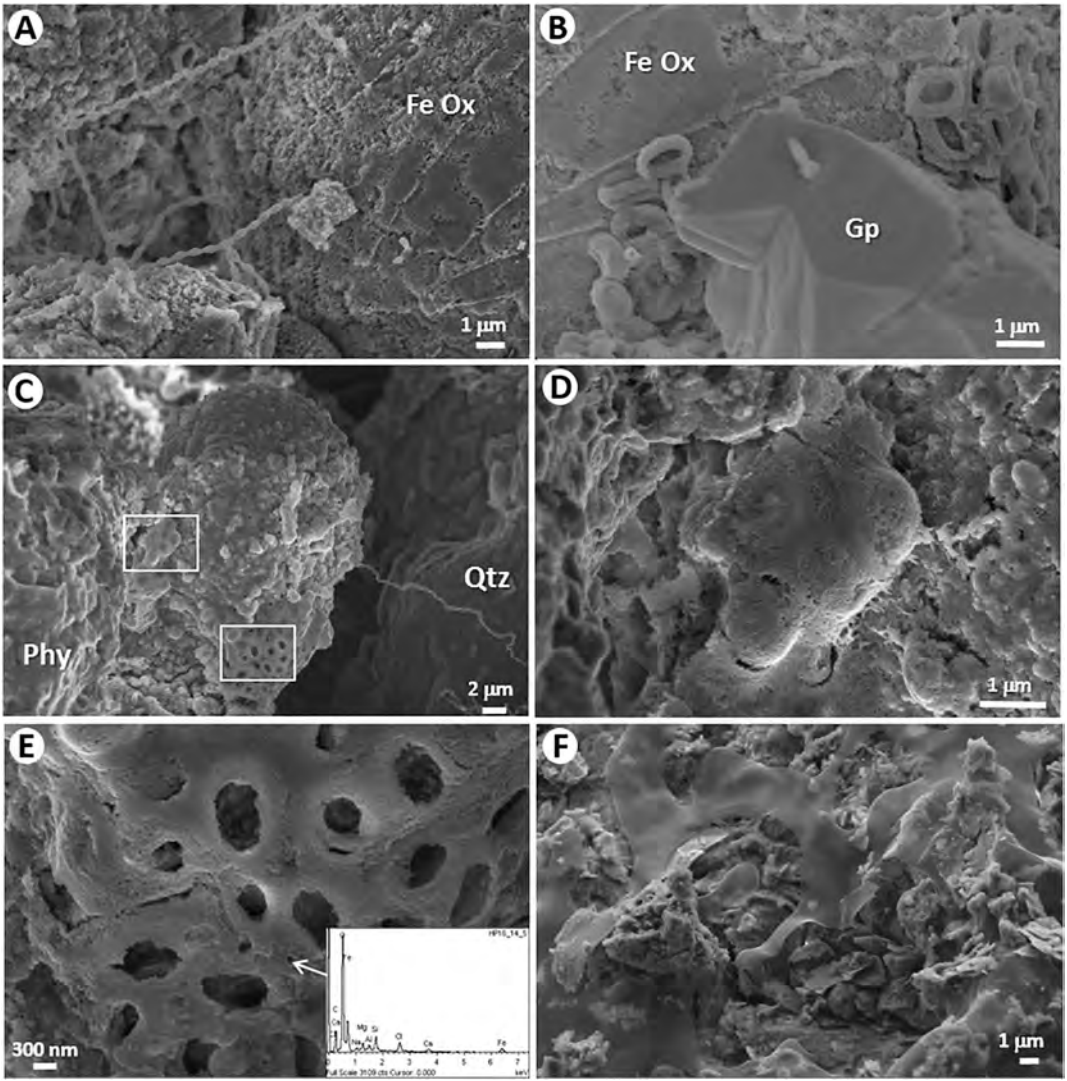

Figure 7

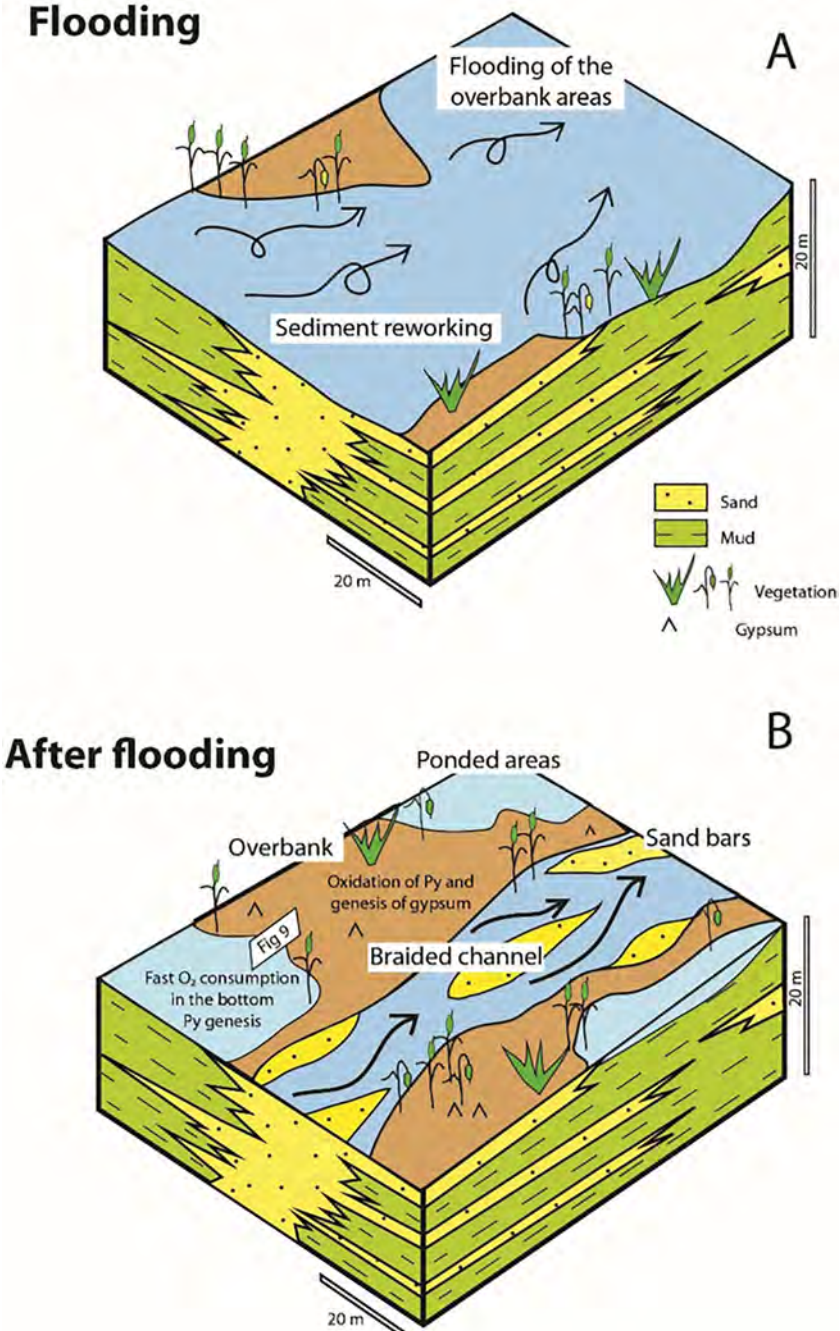
Flooding
A
Flooding of the overbank areas
Sediment reworking
20 m
20 m
Sand
Mud
Vegetation
Gypsum
After flooding
B
Ponded areas
Overbank
Sand bars
Oxidation of Py and genesis of gypsum
Fig 9
Braided channel
Fast O_2 consumption in the bottom Py genesis
20 m
20 m

Figure 8

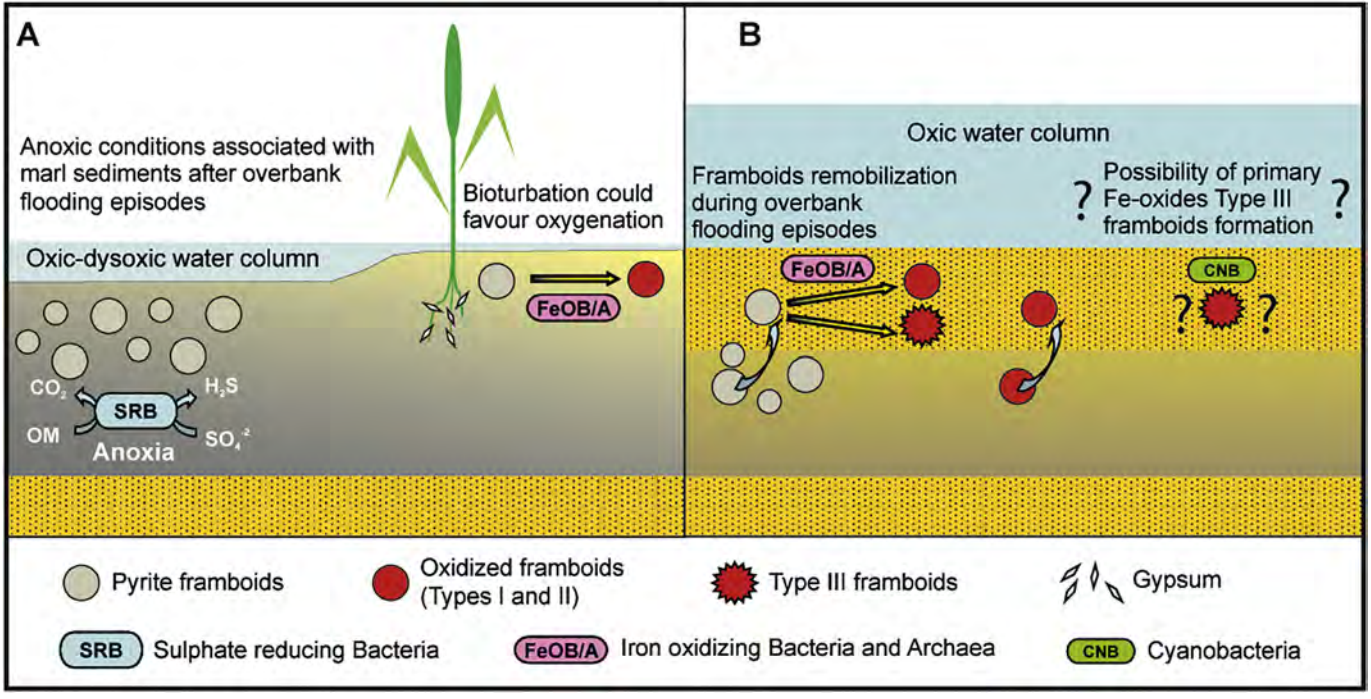
A
Anoxic conditions associated with marl sediments after overbank flooding episodes
Bioturbation could favour oxygenation
Oxic-dysoxic water column
FeOB/A
CO2
H2S
SRB
OM
SO4-2
Anoxia
B
Oxic water column
Framboids remobilization during overbank flooding episodes
?
Possibility of primary Fe-oxides Type III framboids formation
?
FeOB/A
CNB
? ?
Pyrite framboids
Oxidized framboids (Types I and II)
Type III framboids
Gypsum
SRB
Sulphate reducing Bacteria
FeOB/A
Iron oxidizing Bacteria and Archaea
CNB
Cyanobacteria

Figure 9